1. Publication Nº	2. Version	3. Date	5. Distribution
INPE-3915-RPE/510		Jun, 1986	☐ Internal ☒ External ☐ Restricted

4. Origin	Program
DMS/DPL	PCEN

6. Key words - selected by the author(s)

PLASMA PHYSICS
ROTATING PLASMAS
PLASMA CENTRIFUGE
ISOTOPE ENRICHMENT

7. U.D.C.: 533.9

8. Title

INPE-3915-RPE/510

THEORETICAL BEHAVIOR OF FULLY IONIZED MULTIPLE SPECIES MAGNETIZED PLASMAS UNDER ROTATION

10. Nº of pages: 61

11. Last page: 54

12. Revised by

Gerson Otto Ludwig

9. Authorship

J.A. Bittencourt

Responsible author

13. Authorized by

Marco Antonio Raupp
Director General

14. Abstract/Notes

A multiple species fluid model for a fully ionized, magnetized plasma under rotation is described. The basic fluid equations are the continuity and momentum equations for each species, including centrifugal, electromagnetic, pressure gradient and collisional forces, in cylindrical geometry. This model is used to describe the steady state behavior of the fully ionized cylindrical plasma column in a laser-initiated vacuum-arc plasma centrifuge. It is shown that there is a family of theoretically possible dynamical equilibrium configurations, which can be achieved by different combinations of ion rotation velocity, radial ion density distribution and radial dependence of internal electric potential. A numerical analysis is presented which shows the radial distribution and parametric dependences of the various plasma parameters under equilibrium conditions, including the ion separation factor, considering a nickel-copper plasma. The numerical results are analyzed and discussed on light of experimentally measured plasma characteristics in a vacuum-arc plasma centrifuge.

15. Remarks

ABSTRACT

A multiple species fluid model for a fully ionized, magnetized plasma under rotation is described. The basic fluid equations are the continuity and momentum equations for each species, including centrifugal, electromagnetic, pressure gradient and collisional forces, in cylindrical geometry. This model is used to describe the steady state behavior of the fully ionized cylindrical plasma column in a laser-initiated vacuum-arc plasma centrifuge. It is shown that there is a family of theoretically possible dynamical equilibrium configurations, which can be achieved by different combinations of ion rotation velocity, radial ion density distribution and radial dependence of internal electric potential. A numerical analysis is presented which shows the radial distribution and parametric dependences of the various plasma parameters under equilibrium conditions, including the ion separation factor, considering a nickel-copper plasma. The numerical results are analyzed and discussed on light of experimentally measured plasma characteristics in a vacuum-arc plasma centrifuge.

SUMMARY

FIGURE CAPTIONS

Page

1. INTRODUCTION

Centrifugal separation of elements and isotopes in rotating, magnetized plasma columns has been the subject of research for many years. A comprehensive review on this subject, and the research which was done up to 1970, has been presented by Lehnert (1971). This review includes an extensive bibliography of the various investigations and surveys the theoretical considerations and experimental results for partially and fully ionized rotating, magnetized plasmas. It also summarizes the applications of rotating plasmas to nuclear fusion research, cosmical physics and technical devices such as adjustable plasma condensers, plasma guns and propulsion systems. Slepian (1955) was the first to study rotating plasmas as means for isotope enrichment. Bonnevier (1966) suggested the use of a fully ionized plasma centrifuge to enhance the mass separation effect and later studied the plasma centrifuge experimentally (Bonnevier, 1971), where a rotating fully ionized plasma was surrounded by a partially ionized plasma and neutral gas. Afterwards several researchers have studied gas discharge plasma centrifuges and have measured isotopic enrichment in gaseous, rotating plasmas (James and Simpson, 1974, 1978; Heller and Simon, 1974; Kaneko et al., 1978; Brand et al., 1979; Wijnakker and Granneman, 1980).

A gas discharge plasma centrifuge, in its simplest configuration, consists basically of a gas at about 1 Torr pressure in a cylindrical vacuum vessel, immersed in an externally applied uniform axial magnetic field. The gas is partially ionized when current is discharged radially between two concentric cylindrical electrodes. The resulting $\vec{J} \times \vec{B}$ magnetic force density, due to radial current flow across the axial magnetic field, induces the azimuthal plasma rotation. The centrifugal force, acting radially outwards, causes a partial separation of the different ion species in the radial direction. The plasma centrifuge contains no moving mechanical parts, since the rotation is produced by an electromagnetic body force on the plasma and therefore can, in principle, reach much higher rotational velocities than the neutral particles in a mechanical gaseous centrifuge.

In the experiments conducted in either partially ionized or highly ionized rotating plasma colums, which were surrounded by neutral gas, the neutral atom drag on the rotating ions limits the rotational velocity to values below the Alfvēn critical velocity. Alfvēn (1960) has suggested that in a partially ionized plasma a strong enhanced ionization process arises when the directed kinetic energy of the ions, relative to the neutrals, approaches the first ionization energy of the neutrals. Additional energy input then goes selectively, via electrons, into further ionization of the neutrals, so that the ion rotational velocity is limited. Such a limiting critical velocity has been experimentally verified in rotating plasmas. Explanations for the origin of this critical velocity have been proposed by Fahleson (1961), Sockol (1968), Lehnert (1960), and McKenzie and Varma (1981). The deleterious effects of neutral atom viscous dissipation and the Alfvēn limit have resulted in relatively weak isotope enrichments in gas discharge plasma centrifuges.

More recently a new type of plasma centrifuge has been developed (Krishnan et al., 1981; Geva et al., 1981) in which the plasma source is a vacuum-arc triggered by a pulsed laser and discharged between a metallic cathode and a grounded mesh anode at one end of a 1.5m long cylindrical vacuum vessel. Plasma rotation about the cylinder axis is sustained by the self-consistent radial electric field, produced inside the plasma column, crossed with the externally applied uniform axial magnetic field. The plasma produced in the vacuum-arc centrifuge is fully ionized and composed of the cathode material. The ionized particles evaporate from the cathode with large radial and axial velocities, and achieve rigid rotor angular rotation frequencies between 6×10^4 and 3×10^5rad/s (Krishnan et al, 1983). The absence of a neutral gas envelope and its deleterious effects has resulted in isotopic enrichments in a vacuum-arc plasma centrifuge much larger than those measured earlier in a gas discharge centrifuge. Results of element and isotope separation in various carbon and metal plasmas have been presented by Krishnan et al. (1983), and Geva et al. (1984), showing the potential for vacuum-arc plasma centrifuges to serve as practical isotope separators. They found that the centrifugal

separation increases rapidly with distance from the cathode plasma source and reaches an asymptotic value at about 70cm downstream. The observations showed that the separation factor increased exponentially with the square of the radius, the electric potential profile inside the plasma had a parabolic radial dependence and the radial ion density distribution was Gaussian, in agreement with a simple, two-ion species, steady state fluid model of the rotating plasma. An improved matched impedance, low-voltage, vacuum-arc plasma centrifuge, with much better electrical efficiency than a previous prototype centrifuge, has been recently described by Prasad and Krishnan (1986).

A vacuum-arc plasma centrifuge has also been developed at INPE and a preliminary description of the machine was given by Del Bosco and Ludwig (1982). The first experimental results of isotope enrichment, measured using an electric quadrupole mass spectrometer, were presented by Del Bosco et al. (1985), in which an enrichment factor of 167% was obtained for ^{13}C in a carbon plasma. More recently, Del Bosco et al. (1986) have reported an enrichment factor of 392% for ^{13}C.

This paper describes a three-species (electrons and two types of ions) warm fluid model used to analyze the behavior of the magnetized, fully ionized, rotating plasma in a vacuum-arc centrifuge. Initially, in Section 2, a physical picture of the rotating plasma, based on experimental findings, is presented. The region of the arc near the cathode is still poorly understood and attention is focused on the streaming plasma region. The basic set of time-dependent multispecies fluid equations and the relevant electrodynamic equations are described in Section 3 and applied to a cylindrical plasma column under rotation. A reduced set of time-dependent fluid equations with azimuthal symmetry is outlined in Section 4, in which a Lagrangian reference frame moving at the constant axial ion velocity is considered and the electron inertia is neglected. The resulting set of equations is further simplified in Section 5, considering a steady state equilibrium situation with no radial plasma motion and with the plasma

column rotating as a rigid rotor. A detailed analysis of the steady state fluid equations is presented in Section 6, where a family of equilibrium solutions is identified, as there are many theoretically possible equilibrium configurations which can be achieved by different combinations of ion rotation velocity (centrifugal force), radial particle density distribution (pressure gradient force) and radial dependence of internal electric potential (electric force). Limiting equilibrium values of the various parameters and expressions for the separation factor are also discussed. A numerical analysis has been made for the various possible equilibrium configurations of the rotating plasma column and the results are presented and discussed in Section 7. The radial distributions and parametric dependences of the various plasma parameters, including the ion separation factor, are analyzed on light of the experimentally observed plasma behavior in a vacuum-arc centrifuge, considering specifically a nickel (Ni)-copper (Cu) plasma. A summary of the results and conclusions are presented in Section 8.

2. PHYSICAL PICTURE OF THE ROTATING PLASMA COLUMN

The following physical description of the rotating plasma column seems to be appropriate. The fully ionized plasma, composed of the cathode material, emanates from the cathode during the arc discharge and expands into the magnetized vacuum chamber. The electrons are effectively tied to the axial magnetic field lines, since the electron-electron collision frequency, ν_{ee}, is much smaller than the electron cyclotron frequency, Ω_{ce} ($\nu_{ee}/\Omega_{ce} \ll 1$). On the other hand, for the ions $\nu_{ii}/\Omega_{ci} \sim 0.1$ (where ν_{ii} denotes the ion-ion collision frequency and Ω_{ci} the ion cyclotron frequency), resulting in ambipolar radial diffusion in the streaming plasma region and the establishment of a self-consistent internal radial electric field $\vec{E}_r$, which points radially inward. This radial electric field crossed with the axial magnetic induction $\vec{B}_z$ produces an azimuthal electromagnetic plasma drift, whose velocity is given by

$$\vec{u}_\theta = \vec{E}_r \times \vec{B}_z/B^2 \qquad (1)$$

which puts the plasma into rotation about the column axis. The negative radial pressure gradient crossed with the axial magnetic induction generates an azimuthal diamagnetic drift, whose velocity is given by

$$\vec{u}_\theta = -(\vec{\nabla}p)_r \times \vec{B}_z/(n_\alpha q_\alpha B^2) \ . \qquad (2)$$

Thus, this diamagnetic drift adds to the electromagnetic drift for the electrons and opposes to it for the ions, with the result that the electrons rotate faster than the ions. The resulting azimuthal current density is in the direction opposite to that of the azimuthal particle motion, so that the plasma is confined by the associated $\vec{J}_\theta \times \vec{B}_z$ radial force density (see Fig. 1). The centrifugal force, resulting from the plasma rotation, acts radially outward and causes radial separation between particles of different mass/charge ratio. Ion-ion collisions lead to radial ion transport within the confined column, whereas ion-electron collisions lead to gradual diffusion of the quasi-neutral plasma across the magnetic field lines. The rotating fully ionized plasma streams axially towards the end flange and further down the column presumably reaches a quasi-steady state situation in which the net radial flux due to ion-ion collisions is zero, and the different ion species have the same angular rotation frequency. The electron angular rotation frequency, however, is still slightly higher than the ion rotation frequency. The radial density profiles of the various species are not the same and a radial enrichment is achieved in which the heavier ion species are more abundant at large radii than lighter species.

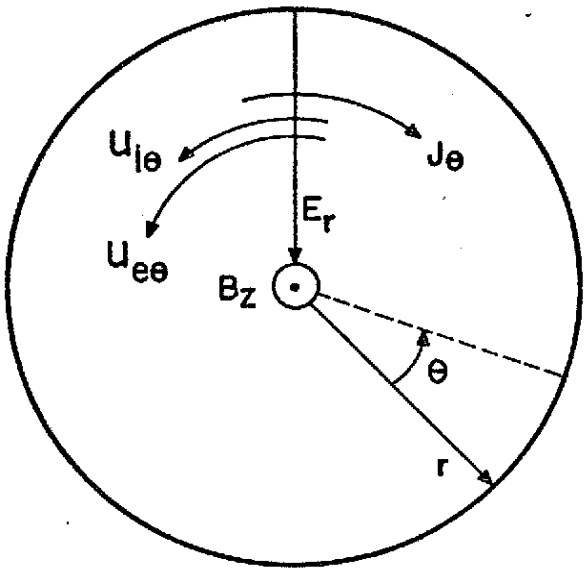

Fig. 1 - Schematic representation of the rotating plasma in the (r,θ) plane showing the relative orientations of the electric and magnetic fields, the particle azimuthal rotation velocities and the azimuthal current density.

Measurements performed by Geva et al. (1984) in a vacuum-arc fully ionized plasma centrifuge revealed the following typical values of the plasma parameters: peak (on axis) ion density $n_i \sim 10^{13}cm^{-3}$, full width at half maximum radius of a Gaussian radial density profile of 2.5cm, axial drift velocity $u_z \sim 10^6cm/s$, mean average charge $\langle Z \rangle = 3$ for a cooper/nickel plasma mixture, transit time through the column of 160-300μs, rigid rotor angular rotation frequencies between 6×10^4 and $3 \times 10^5 rad/s$, and estimated temperature of 1eV. In a more recent work, using an improved low-voltage vacuum-arc centrifuge, Prasad and Krishnan (1986) measured typical values of $n_e \sim 10^{15}cm^{-3}$ and $T_i \sim 3eV$. For typical plasma parameters of $n_e \sim 10^{13}cm^{-3}$, $\langle Z \rangle = 3$, $T_e = T_i = 1eV$ and $B = 0.2T$, estimated values of various length and frequency scales of interest are as follows: Debye length $\lambda_D \sim 10^{-4}cm$, electron gyrofrequency $\Omega_{ce} \sim 10^{10}rad/s$, electron gyroradius $r_e \sim 10^{-3}cm$, ion gyrofrequency $\Omega_{ci} \sim 10^6 rad/s$, ion gyroradius $r_i \sim 10^{-1}cm$, ion axial velocity $u_z \sim 10^6 cm/s$, ion-ion collision frequency $\nu_{ii} \sim 10^6 - 10^7 s^{-1}$, and ion-ion collision mean free

path $\lambda_{ii} \sim 0.1$ - 1cm. Thus, the gyroradii and collisional mean free paths are much smaller than the typical plasma column dimensions (length of about one meter and radius of a few centimeters). Also, a few rotation orbits (about five) and many collisions (of order 10^2) are experienced by a typical plasma element during its time of transit axially down the column.

3. FLUID MODEL OF A MULTISPECIES ROTATING PLASMA

The basic set of fluid equations describing a multispecies warm plasma includes the equations of continuity, momentum and energy for each particle species.

Denoting the particle number density and the macroscopic fluid velocity of the α species by $n_\alpha(\vec{r},t)$ and $\vec{u}_\alpha(\vec{r},t)$, respectively, the continuity equation can be expressed as

$$\frac{\partial}{\partial t} n_\alpha + \vec{\nabla} \cdot (n_\alpha \vec{u}_\alpha) = P_\alpha - L_\alpha \ , \tag{3}$$

where P_α and L_α represent, respectively, the time rate of production and loss of the type α species per unit volume. The production and loss terms can be neglected when (3) is applied to regions which do not include the sources of type α particles (e.g. the cathode, in the case of the vacuum-arc centrifuge), and for time scales in which the recombination processes are not important.

Including the effects of rotational, electromagnetic, pressure gradient and collisional forces, the momentum equation for the α species can be written, in the inertial laboratory frame, as

$$m_\alpha \left(\frac{\partial}{\partial t} + \vec{u}_\alpha \cdot \vec{\nabla} \right) \vec{u}_\alpha = Z_\alpha e(\vec{E} + \vec{u}_\alpha \times \vec{B}) - \frac{1}{n_\alpha} \vec{\nabla} p_\alpha - m_\alpha \sum_\beta \nu_{\alpha\beta} (\vec{u}_\alpha - \vec{u}_\beta), \tag{4}$$

where m_α denotes the particle mass, $Z_\alpha e$ is the particle charge, $\vec{E}$ is the electric field, $\vec{B}$ is the magnetic induction, p_α is the partial

kinetic pressure (assumed to be isotropic) and $\nu_{\alpha\beta}$ is the momentum transfer collision frequency between the α and β species.

Equations (3) and (4) must be complemented by an appropriate energy conservation equation relating $p_\alpha(\vec{r},t)$ with $n_\alpha(\vec{r},t)$ and $\vec{u}_\alpha(\vec{r},t)$. However, assuming a constant and uniform temperature T_α throughout the plasma it is sufficient to use the ideal gas equation of state,

$$p_\alpha = n_\alpha k T_\alpha \ , \tag{5}$$

where k is Boltzmann's constant.

The internal self-consistent electrostatic field $\vec{E}(\vec{r},t)$ can be expressed in terms of the electric potential $\phi(\vec{r},t)$ through the equation

$$\vec{E} = -\vec{\nabla}\phi \ , \tag{6}$$

where $\phi(\vec{r},t)$ satisfies Poisson equation inside the plasma,

$$\nabla^2\phi = -\frac{\rho}{\varepsilon_0} \ , \tag{7}$$

and where the electric charge density is given by

$$\rho = e\sum_\alpha Z_\alpha n_\alpha \ . \tag{8}$$

The magnetic induction produced by currents and time-dependent electric fields inside the rotating plasma can be considered to be much smaller than the externally applied axial $\vec{B}$ field. Therefore, Ampere's law is not considered here and the magnetic induction appearing in the momentum equation (4) is due only to the externally applied field.

Eliminating $p_\alpha(\vec{r},t)$, $\vec{E}(\vec{r},t)$ and $\rho(\vec{r},t)$ from these equations, and neglecting the production and loss terms, we obtain the following set of equations for the type α species,

$$\frac{\partial}{\partial t}n_\alpha + \vec{\nabla}\cdot(n_\alpha\vec{u}_\alpha) = 0 \ , \tag{9}$$

$$m_\alpha\left(\frac{\partial}{\partial t}+\vec{u}_\alpha\cdot\vec{\nabla}\right)\vec{u}_\alpha = Z_\alpha e(-\vec{\nabla}\phi+\vec{u}_\alpha\times\vec{B}) - \frac{kT_\alpha}{n_\alpha}\vec{\nabla}n_\alpha - m_\alpha\sum_\beta\nu_{\alpha\beta}(\vec{u}_\alpha-\vec{u}_\beta) \ , \tag{10}$$

$$\nabla^2\phi = -\frac{e}{\varepsilon_0}\sum_\alpha Z_\alpha n_\alpha \ . \tag{11}$$

If the number of different species considered is denoted by a, then (4a + 1) scalar equations coupled through the collisional term and through Poisson equation will have to be solved simultaneously in order to determine the variables n_α, $u_{\alpha i}$ (i = 1, 2, 3) and ϕ, with $\alpha = 1, 2, \ldots, a$.

To apply this closed set of equations to a multispecies rotating magnetized plasma in cylindrical geometry, consider a cylindrical column of plasma rotating about the z-axis, immersed in a constant axial magnetic induction $\vec{B} = B\hat{z}$. In cylindrical coordinates (r, θ, z), (9) becomes

$$\frac{\partial}{\partial t}n_\alpha + \frac{1}{r}\frac{\partial}{\partial r}(rn_\alpha u_{\alpha r}) + \frac{1}{r}\frac{\partial}{\partial\theta}(n_\alpha u_{\alpha\theta}) + \frac{\partial}{\partial z}(n_\alpha u_{\alpha z}) = 0 \ , \tag{12}$$

whereas (10) can be separated in an r-component equation,

$$m_\alpha\left(\frac{D}{Dt}u_{\alpha r} - \frac{u_{\alpha\theta}^2}{r}\right) = Z_\alpha e(E_r + u_{\alpha\theta}B) - kT_\alpha\frac{\partial}{\partial r}\ell n(n_\alpha) - m_\alpha\sum_\beta\nu_{\alpha\beta}(u_{\alpha r}-u_{\beta r}) \tag{13}$$

a θ-component equation,

$$m_\alpha\left(\frac{D}{Dt}u_{\alpha\theta} + \frac{u_{\alpha\theta}u_{\alpha r}}{r}\right) = Z_\alpha e(E_\theta - u_{\alpha r}B) - kT_\alpha\frac{1}{r}\frac{\partial}{\partial\theta}\ell n(n_\alpha) - m_\alpha\sum_\beta\nu_{\alpha\beta}(u_{\alpha\theta}-u_{\beta\theta}), \tag{14}$$

and a z-component equation,

$$m_\alpha \frac{D}{Dt} u_{\alpha z} = Z_\alpha e E_z - kT_\alpha \frac{\partial}{\partial z} \ell n(n_\alpha) - m_\alpha \sum_\beta \nu_{\alpha\beta}(u_{\alpha z} - u_{\beta z}) \ , \qquad (15)$$

where D/Dt denotes the total or substantial time derivative,

$$\frac{D}{Dt} = \frac{\partial}{\partial t} + u_{\alpha r} \frac{\partial}{\partial r} + u_{\alpha\theta} \frac{1}{r} \frac{\partial}{\partial \theta} + u_{\alpha z} \frac{\partial}{\partial z} \ . \qquad (16)$$

Poisson equation (11) becomes, in cylindrical coordinates,

$$\frac{1}{r} \frac{\partial}{\partial r}\left(r \frac{\partial \phi}{\partial r}\right) + \frac{1}{r^2} \frac{\partial^2 \phi}{\partial \theta^2} + \frac{\partial^2 \phi}{\partial z^2} = - \frac{e}{\varepsilon_0} \sum_\alpha Z_\alpha n_\alpha \ . \qquad (17)$$

For a fully ionized plasma with three particle species (electrons and two types of ions), (12) to (17) with $\alpha = 1, 2, 3$ constitute a complete set of coupled nonlinear partial differential equations for the unknowns n_α, $u_{\alpha r}$, $u_{\alpha\theta}$, $u_{\alpha z}$ and ϕ. These equations must be solved simultaneously under proper initial and boundary conditions in cylindrical geometry.

When the plasma density is relatively high and/or the internal electrostatic potential relatively small, it becomes inconvenient to look for a numerical solution of Poisson equation, since the total charge density ρ required to produce the electrostatic potential ϕ becomes an extremelly small fraction of the electron (or ion) charge density $Z_\alpha e n_\alpha$. This is the situation in the bulk part of the rotating high-density plasma in the vacuum-arc centrifuge, where $n_e \simeq 10^{13} cm^{-3}$ (Geva et al., 1984). In this case, instead of solving Poisson equation numerically, it is appropriate to consider the plasma quasi-neutrality condition

$$\sum_\alpha Z_\alpha n_\alpha = 0 \ , \qquad (18)$$

even though there is an internal self-consistent electrostatic field in the bulk part of the plasma. Therefore, instead of solving Poisson equation, the electric potential can be calculated using the fluid equations together with (18). This approximation is adequate as long as the plasma density is sufficiently high and/or the electrostatic potential sufficiently small, but it certainly breaks down in the plasma sheath region near the boundaries of the rotating plasma column.

4. REDUCED SET OF TIME-DEPENDENT FLUID EQUATIONS

In order to simplify this set of equations some assumptions will be made.

The rotating plasma column is assumed to be azimuthally symmetric, so that all variables are independent of θ (all θ-derivatives vanish). In this case, $\vec{E}_\theta = 0$, as required by the Maxwell equation $\vec{\nabla} \times \vec{E} = 0$, considering $\vec{B}$ constant.

For regions not too close to the source of plasma particles (cathode), it is experimentally justified (Geva et al., 1984) to consider the axial velocity $u_{\alpha z}$ to be constant. In this case, $Du_{\alpha z}/Dt = 0$. If a longitudinal current flows in the plasma, then the electrons must be moving relative to the ions, along the z-axis, so that $u_{ez} \neq u_{iz}$, although u_{iz} ($i = 1, 2$) can be considered to be the same for the ion species. Geva et al. (1984) experimentally observed a constant axial ion drift velocity $u_{iz} \simeq 10^6$cm/s (with slightly different values for different types of plasmas), independent of radial and axial location inside the plasma column. Also, according to Geva et al. (1984), the axial electric field is of the order of 1V/m, much smaller than the radial electrostatic field (of the order of 10^3V/m). Therefore, the particle number densities depend much more strongly on r than on z.

If J_z denotes the longitudinal current density, then

$$J_z = -en_e(u_{ez} - u_{iz}) \ , \tag{19}$$

where the charge neutrality condition $n_e = Z_1 n_1 + Z_2 n_2$, with $u_{1z} = u_{2z}$, has been used.

Also, considering time scales appropriate to analyze the ion motion, electron inertia can be neglected.

Furthermore, it is convenient to consider a Lagrangian reference frame moving at the constant axial ion velocity u_{iz}. Thus, a total or substantial time derivative is defined according to

$$\frac{d}{dt} = \frac{\partial}{\partial t} + u_{iz} \frac{\partial}{\partial z} \, . \tag{20}$$

In this axially moving reference frame all ion motions occur in the (r,θ) plane and, consequently, all ion variables become explicit functions of only r and t (with azimuthal symmetry). The small z-dependence is intrinsically incorporated in the time-dependence seen in this moving frame and the boundary conditions specified at $z = z_0$ can be considered as initial conditions at $t = t_0$.

Therefore, with these assumptions, the continuity equation (12) for the electrons becomes, using (19),

$$\frac{d}{dt} n_e - \frac{J_z}{e n_e} \frac{\partial}{\partial z} n_e + \frac{1}{r} \frac{\partial}{\partial r} (r n_e u_{er}) = 0 \tag{21}$$

and for the ions (i = 1, 2),

$$\frac{d}{dt} n_i + \frac{1}{r} \frac{\partial}{\partial r} (r n_i u_{ir}) = 0 \, . \tag{22}$$

Neglecting electron inertia, the r-component momentum equation (13) for the electrons reduces to

$$-e(E_r + u_{e\theta} B) - kT_e \frac{\partial}{\partial r} \ell n(n_e) = 0 \, , \tag{23}$$

whereas the θ-component momentum equation (14) yields

$$u_{er} = 0 \ . \tag{24}$$

The electrons are therefore tightly coupled to the longitudinal magnetic field lines. In view of (24) the continuity equation (21) for the electrons reduces further to

$$\frac{d}{dt} n_e - \frac{J_z}{e n_e} \frac{\partial}{\partial z} n_e = 0 \ . \tag{25}$$

If no axial current flows through the plasma column ($J_z = 0$), then (25) yields a constant electron number density in the axially moving frame ($dn_e/dt = 0$).

The z-component momentum equation (15) for the electrons becomes

$$-eE_z - kT_e \frac{\partial}{\partial z} \ell n(n_e) = 0 \ . \tag{26}$$

so that the electron number density varies longitudinally according to the Boltzmann factor,

$$n_e(r,z,t) = n_e(r,z_0,t) \exp \left\{ \frac{e}{kT_e} [\phi(r,z,t) - \phi(r,z_0,t)] \right\} \ . \tag{27}$$

For the ions ($i = 1, 2$), the r-component momentum equation (13) can be written as

$$\frac{d}{dt} u_{ir} - u_{ir} \frac{\partial}{\partial r} u_{ir} - \frac{u_{i\theta}^2}{r} = \frac{Z_{ie}}{m_i} (E_r + u_{i\theta} B) - \frac{kT_i}{m_i} \frac{\partial}{\partial r} \ell n(n_i) -$$

$$- \sum_j \nu_{ij} (u_{ir} - u_{jr}) \tag{28}$$

and the θ-component momentum equation (14) as

$$\frac{d}{dt}u_{i\theta} + u_{ir}\frac{\partial}{\partial r}u_{i\theta} + \frac{u_{i\theta}u_{ir}}{r} = -\frac{Z_i e}{m_i}u_{ir}B - \sum_j \nu_{ij}(u_{i\theta} - u_{j\theta}) \ . \qquad (29)$$

Note that these last two equations do not depend explicitly on z, since the z-dependence has been intrinsically incorporated in the time-dependence seen in the axially moving frame of reference. The z-component momentum equation (15) is therefore decoupled from (28) and (29), and reads

$$\frac{Z_i e}{m_i}E_z - \frac{kT_i}{m_i}\frac{\partial}{\partial z}\ell n(n_i) = 0 \ , \qquad (30)$$

since u_{iz} is considered constant and $u_{1z} = u_{2z}$. Therefore, the ion number densities also vary longitudinally according to the Boltzmann factor,

$$n_i(r,z,t) = n_i(r,z_0,t)\ \exp\left\{-\frac{Z_i e}{kT_i}[\phi(r,z,t) - \phi(r,z_0,t)]\right\} \ . \qquad (31)$$

As stated before, the particle number densities depend much more strongly on r than on z, since the axial electric field is much smaller than the radial electrostatic field.

The original closed set of coupled nonlinear partial differential equations (12) to (18) has now been reduced to a closed set involving the variables n_α, u_{ir}, $u_{\alpha\theta}$ and ϕ, with α denoting electrons and two ion species ($i = 1, 2$).

5. STEADY STATE FLUID EQUATIONS

From the experimentally observed axial evolution of the radial profiles of the plasma density and of the separation factor, it is seen that the plasma approaches a quasi-equilibrium state during its

time of transit through the column. According to Geva et al. (1984), the plasma emanates from the cathode and streams axially downstream to the end of the column with a transit time which varies between 160μs to 300μs. In this quasi-equilibrium region the changes with respect to z are smaller than over comparable intervals in the region closer to the cathode, and the radial velocity components are much smaller than the other ones.

It has also been shown experimentally that the plasma rotates as a rigid body in its bulk part (except, perhaps, in the sheath region), so that

$$u_{\alpha\theta} = \omega_{\alpha} r \ , \tag{32}$$

where ω_{α} denotes the angular rotation frequency of the α species. Under steady state equilibrium it is expected that the different ions, at each radial position, have achieved the same rotational velocity ($u_{1\theta} = u_{2\theta}$). The ion-ion collisions are responsible for this equalization of the azimuthal rotational velocities of the different ion species (assuming negligible electron inertia), under equilibrium conditions. At the same time, the steady state condition is assumed to hold on a time scale in which kinetic energy damping due to ion-ion collisions is not significant. The electrons, of course, may have an azimuthal rotational velocity $u_{e\theta}$ higher than that of the ions, in order to provide a confining $\vec{J}_{\theta} \times \vec{B}$ radial force density.

In what follows it is considered an isothermal cylindrical column of plasma rotating as a rigid body under steady state conditions, with no axial dependence (infinitely long column), and with no boundary conditions involved. Thus, the plasma is uncoupled from the cathode, the anode mesh and the walls, so that their effects are not considered.

Therefore, assuming that the plasma has reached a steady state equilibrium in a region far from the cathode, with no z-

dependence, the ion continuity equation (22) yields

$$u_{ir} = 0 \ , \tag{33}$$

since there is no spatial source of plasma particles to allow for a nonvanishing radial plasma flux. Hence, the plasma only rotates in the θ-direction in the axially moving frame, under the presence of the internal self-consistent radial electric field due to charge separation. The azimuthal diamagnetic current $\vec{J}_\theta$ due to the differential motion of electrons and ions, crossed with the magnetic field, provides the radial confining force on a fluid element against the centrifugal force and the pressure gradient force, which act radially outwards.

The r-component momentum equation (28) for the ions becomes, under these conditions,

$$m_i \frac{u_{i\theta}^2}{r} + Z_i e(E_r + u_{i\theta}B) - kT_i \frac{\partial}{\partial r} \ell n(n_i) = 0 \ , \tag{34}$$

whereas the θ-component momentum equation (29) gives no information, since $u_{ir} = 0$.

For the electrons, the momentum equation to be considered is (23), which is similar to (34) except for the vanishing electron inertia.

Equations (34) and (23), together with the macroscopic plasma neutrality approximation (18), constitute therefore a set of equations which describe the steady state behavior of an isothermal, multispecies, magnetized plasma rotating as a solid body, with no z-dependence and no radial plasma flow.

6. ANALYSIS OF STEADY STATE FLUID EQUATIONS

Using the rigid rotor condition (32), Eqs. (23) and (34) can be recast as

$$-e(E_r + \omega_e rB) - kT_e \frac{\partial}{\partial r} \ell n(n_e) = 0 \ , \tag{35}$$

$$m_i \omega_i^2 r + Z_i e(E_r + \omega_i rB) - kT_i \frac{\partial}{\partial r} \ell n(n_i) = 0 \ , \tag{36}$$

with $i = 1, 2$. These equations involve the variables ω_e, ω_i, $E_r(r)$, $n_e(r)$ and $n_i(r)$, where it is assumed that $\omega_1 = \omega_2$, as discussed in section 5. Furthermore, the radial electric field can be expressed in terms of the internal plasma potential $\phi(r)$ as

$$E_r(r) = - \frac{\partial}{\partial r} \phi(r) \ , \tag{37}$$

A family of equilibrium solutions is obtained from (35) and (36), together with the plasma neutrality approximation (18). A parametric numerical analysis can be made, for example, ω_i and $E_r(r)$ can be specified, and (36) used to determine $n_i(r)$, for $i = 1, 2$. The plasma neutrality approximation then yields $n_e(r)$, which allows the calculation of ω_e from (35). From (35) and (36) explicit expressions for $n_e(r)$ and $n_i(r)$ can be written in terms of the other variables as

$$n_e(r) = n_e(0) \exp \left[- \frac{e}{kT_e} \int_0^r E_r dr - \frac{e\omega_e B r^2}{2kT_e} \right] \ , \tag{38}$$

$$n_i(r) = n_i(0) \exp \left[\frac{Z_i e}{kT_i} \int_0^r E_r dr + \frac{m_i \omega_i}{2kT_i} (\omega_i + \Omega_{ci}) r^2 \right] \ , \tag{39}$$

where $\Omega_{ci} = Z_i eB/m_i$ denotes the ion cyclotron frequency.

Useful information can be further obtained from (35) and (36) by solving them explicitly in terms of the rotational frequencies. From (35) it is obtained, for the electrons,

$$\omega_e = \frac{1}{r} \left[- \frac{E_r}{B} - \frac{kT_e}{eB} \frac{\partial}{\partial r} \ell n(n_e) \right] \ , \tag{40}$$

showing that the electron rotation frequency is due to the electromagnetic $\vec{E} \times \vec{B}$ drift velocity plus the diamagnetic $\vec{\nabla} p_e \times \vec{B}$ drift velocity. Note that these two velocities are both in the positive θ-direction for an electric field and a pressure gradient pointing radially inwards (confined plasma). Furthermore, for a rigid rotor ω_e must be constant, which implies that E_r must be proportional to r and $\ell n(n_e)$ must be proportional to r^2. Therefore,

$$\vec{E}_r(r) = E_r \hat{r} = -ar\hat{r} \quad (a > 0) \ , \tag{41}$$

$$\phi(r) - \phi(0) = \frac{a}{2} r^2 \ , \tag{42}$$

$$n_e(r) = n_e(0) \exp\left(-\beta_e r^2\right) \ , \tag{43}$$

where a and β_e are constants, so that the electric field varies linearly with r, the electric potential shows a parabolic radial profile and the electron number density achieves a Gaussian radial distribution accross the column, with β_e given by

$$\beta_e = \frac{e}{2kT_e}(\omega_e B - a) \ . \tag{44}$$

Note that, since $a > 0$, the condition $\omega_e > a/B$, or equivalently,

$$u_{e\theta} = \omega_e r > - E_r/B \tag{45}$$

must be satisfied for confinement (i.e. $\partial n_e(r)/\partial r < 0$). Otherwise, $\partial n_e(r)/\partial r \geq 0$. Thus, the electrons must rotate faster than the electromagnetic drift rotation velocity.

Eq. (36) for the ions can be rewritten as

$$\omega_i^2 + \Omega_{ci}\omega_i + \Omega_{ci} \frac{E_r}{rB} - \frac{kT_i}{m_i r} \frac{\partial}{\partial r} \ell n(n_i) = 0 \tag{46}$$

and solving explicitly for the ion rotation frequency,

$$\omega_i = \frac{1}{2}\Omega_{ci}\left\{-1 \pm \left[1 - \frac{4E_r/B}{\Omega_{ci}r} + \frac{4kT_i}{m_i\Omega_{ci}^2 r}\frac{\partial}{\partial r}\ell n(n_i)\right]^{1/2}\right\} . \tag{47}$$

This result also shows that for rigid body rotation (constant ω_i) E_r must be proportional to r and $\ell n(n_i)$ must be proportional to r^2. Thus, using (41) and (42) the ion number density also achieves a Gaussian radial distribution

$$n_i(r) = n_i(0)\exp(-\beta_i r^2) \tag{48}$$

with the constant β_i given by

$$\beta_i = \frac{Z_i e}{2kT_i}\left[a - \omega_i B\left(1 + \frac{\omega_i}{\Omega_{ci}}\right)\right] . \tag{49}$$

For confinement (i.e. $\partial n_i(r)/\partial r < 0$) the following condition must hold,

$$a > \omega_i B\left(1 + \frac{\omega_i}{\Omega_{ci}}\right) \tag{50}$$

which can be rearranged in the form

$$u_{i\theta} = \omega_i r < -\frac{E_r/B}{(1+\omega_i/\Omega_{ci})} . \tag{51}$$

Thus, the ions rotate at a velocity which is smaller than the electromagnetic drift rotation velocity, for confinement. It should be also noted, from (47), that the diamagnetic $\vec{\nabla}p_i \times \vec{B}$ drift velocity for the ions is opposite to the electromagnetic $\vec{E} \times \vec{B}$ drift velocity, considering that the electric field and the pressure gradient point radially inwards. This differential rotation velocity between electrons and ions provides the $\vec{J}_\theta \times \vec{B}$ confining radial force density.

Eq. (47) also shows the existence of two families of solutions for ω_i. The family with the minus sign can be discarded on physical grounds, since ω_i is always expected to be positive (in the θ-direction). During the expansion phase of the plasma, as soon as it is generated at the cathode, the electrons tend to remain tied to the magnetic field lines so that their transverse motion is inhibited due to the negligibly small electron inertia, whereas the ions tend to diffuse across the field lines, thus generating a transverse polarization electric field due to charge separation, which points radially inward. This electric field, crossed with the axial magnetic field, induces the plasma rotation in the positive θ-direction.

It must be also noted that the family of solutions with negative ω_i implies a strongly diamagnetic equilibrium, with a large azimuthal current density and greatly compressed plasma column.

The family of solutions with the plus sign in (47) also has a branch in which ω_i is still negative and therefore physically unacceptable. Eq. (47), with the plus sign, can be rewritten as

$$\omega_i = \frac{1}{2}\,\Omega_{ci}(-1 + D^{1/2}) \ , \tag{52}$$

where D denotes the discriminant

$$D = 1 - \frac{4E_r/B}{\Omega_{ci} r} + \frac{4kT_i}{m_i \Omega_{ci}^2 r}\,\frac{\partial}{\partial r}\ell n(n_i) \ . \tag{53}$$

For real solutions it is required $D \geq 0$, whereas for positive ω_i it is required $D \geq 1$. This situation is illustrated in Fig. 2, where ω_i is plotted as a function of $D^{1/2}$. The full line indicates the solution with the plus sign and the dashed line indicates the solution with the minus sign. Only the part of the solution with the plus sign which has $D \geq 1$ is physically acceptable. Therefore,

$$1 - \frac{4E_r/B}{\Omega_{ci}r} + \frac{4kT_i}{m_i\Omega_{ci}^2 r}\frac{\partial}{\partial r}\ell n(n_i) \geq 1 \tag{54}$$

or, rearranging,

$$n_i(r) \geq n_i(0)\ \exp\left(\frac{m_i\Omega_{ci}}{kT_iB}\int_0^r E_r dr\right) . \tag{55}$$

Using (41) and the expression for Ω_{ci},

$$n_i(r) \geq n_i(0)\ \exp\left(-\frac{Z_i ea}{2kT_i}r^2\right) . \tag{56}$$

Note that $\phi(r) - \phi(0) = ar^2/2$. The equal sign corresponds to the limit of no-rotation, so that this result can be also obtained directly from (34) taking $u_{i\theta} = 0$. Eq. (56) shows that for each electric potential radial curve there corresponds a minimum Gaussian density radial distribution which gives the no-rotation limit. The parametric curves for all positive values of the angular rotation frequency ω_i must yield Gaussian radial density distributions which lie above this lower limiting Gaussian curve. Furthermore, for confined plasmas (with $\beta_i > 0$) the upper limit given in (51) for the rotational velocity must be observed. The angular rotation frequency ω_i corresponding to $\beta_i = 0$ (uniform plasma with vanishing radial pressure gradient) can be obtained from (51) or (47) as

$$\omega_i = \frac{1}{2}\Omega_{ci}\left[-1 + \left(1 - \frac{4E_r/B}{\Omega_{ci}r}\right)^{1/2}\right] \tag{57}$$

or, using (41),

$$\omega_i = \frac{1}{2}\Omega_{ci}\left[-1 + \left(1 + \frac{4a/B}{\Omega_{ci}}\right)^{1/2}\right] . \tag{58}$$

It is seen from (57) that if $|E_r|/B \ll \Omega_{ci} r/4$, then the square root term can be expanded in a Taylor series with the result

$$\omega_i = -\frac{E_r/B}{r} - \frac{(E_r/B)^2}{\Omega_{ci} r^2} + \cdots \tag{59}$$

or, using (6.7),

$$\omega_i = a/B - \frac{(a/B)^2}{\Omega_{ci}} \quad . \tag{60}$$

Thus, to lowest order, the upper limit of ω_i is given by $\vec{E} \times \vec{B}$ angular rotation velocity ($\omega_i = a/B$).

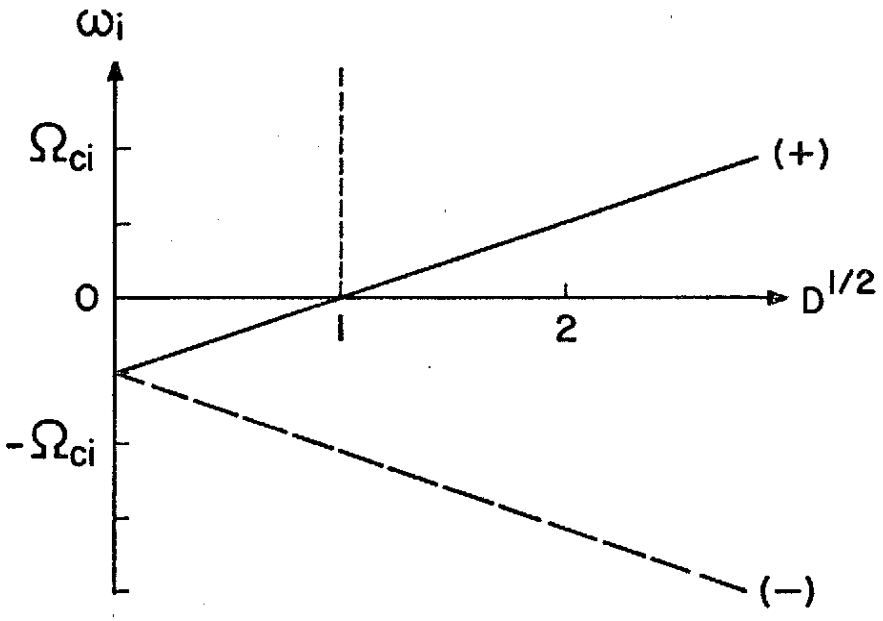

Fig. 2 - Plot of ω_i as a function of $D^{1/2}$, from (52), indicating the physically acceptable family of solutions which have $D \geq 1$ and $\omega_i \geq 0$.

For purposes of element or isotope separation analysis it is appropriate to define a separation factor α_0 between any two ion species as

$$\alpha_0(r) = \frac{n_i(r)/n_j(r)}{n_i(0)/n_j(0)} \cdot \tag{61}$$

For a rigid rotor equilibrium with the ion densities given by (39), the separation factor becomes

$$\alpha_0(r) = \exp(-\beta_i r^2)/\exp(-\beta_j r^2) ,$$

$$= \exp\left\{\frac{r^2}{2k}\left[e\left(\frac{Z_i}{T_i} - \frac{Z_j}{T_j}\right)(\omega B - a) + \omega^2\left(\frac{m_i}{T_i} - \frac{m_j}{T_j}\right)\right]\right\} , \tag{62}$$

where $\omega_i = \omega_j = \omega$. If both ions have the same temperature ($T_i = T_j = T$), then

$$\alpha_0(r) = \exp\left\{\frac{r^2}{2kT}[e(Z_i - Z_j)(\omega B - a) + \omega^2(m_i - m_j)]\right\} . \tag{63}$$

Furthermore, if $Z_i = Z_j$, then the separation factor reduces to

$$\alpha_0(r) = \exp\left[\frac{(m_i - m_j)\omega^2 r^2}{2kT}\right] \tag{64}$$

which is identical to the expression for the separation factor of a gaseous centrifuge. When $Z_i \neq Z_j$, a modified separation factor α can be defined as

$$\alpha(r) = \frac{[n_i(r)]^{1/Z_i}/[n_j(r)]^{1/Z_j}}{[n_i(0)]^{1/Z_i}/[n_j(0)]^{1/Z_j}} \cdot$$

$$= \exp\left[\left(\frac{m_i}{Z_i} - \frac{m_j}{Z_j}\right)\frac{\omega^2 r^2}{2kT}\right] \cdot \tag{65}$$

Thus, the radial potential difference across the column is conveniently eliminated, so that it does not appear in this expression for the modified separation factor.

As a final remark in this analysis, it is to be noted that, since the rigid rotor condition implies Gaussian density radial distributions for the ions and electrons, as well as a parabolic radial profile for the electric potential, another approximation is involved when using the plasma neutrality condition (18) together with the rigid rotor assumption (32). This approximation is reasonable as long as the Gaussian density radial distributions for the ions do not differ significantly from one another, so that their sum is still approximately Gaussian.

7. RESULTS AND DISCUSSION

A parametric analysis has been made for the steady state equilibrium of a multispecies, fully ionized, rotating plasma column composed of ions of Ni and Cu, whose atomic weights are 58.70 and 63.55, respectively. The numerical results presented and discussed in this section are for a 50% Ni and 50% Cu plasma mixture, although any other type of fully ionized plasma could have been considered, including an isotopic mixture of the same element for purposes of isotope separation analysis. Results are presented for singly ionized ions, as well as for triply ionized ions, since Geva et al. (1984) found a mean charge $\langle Z \rangle = 3$ for both Ni and Cu. Various strengths of the magnetic field intensity were considered in order to investigate the effect of the magnetic field on the plasma parameters and separation factor. Values used for the particle number densities at the column axis were $n_1 = n_2 = 10^{13}cm^{-3}$ and $n_e = 2 \times 10^{13}cm^{-3}$ (case of singly ionized ions) or $n_e = 6 \times 10^{13}cm^{-3}$ (case of triply ionized ions), which are typical experimental values according to Geva et al. (1984). The electron and ion temperatures were assumed to be the same and equal to 10^4K. The limiting radial distance was taken as $R_0 = 10cm$ and the radial electric potential differences were specified between the column axis ($r = 0$) and R_0, i.e.,

$$\Delta\phi = \phi(0) - \phi(R_0) \ , \qquad (66)$$

where $\phi(r)$ has a parabolic radial dependence according to (42). Thus, $\Delta\phi$ is always negative.

A family of equilibrium solutions, obtained from (35), (36) and (18), is presented in Fig. 3, which shows the radial distribution of the heaviest ion (Cu) number density for various values of the ion angular rotation frequency ω_i (in units of 10^4Hz) as parameter and for various values of the electric potential difference $\Delta\phi$, as defined in (66), considering B = 0.2T and $Z_1 = Z_2 = 1$. Important points to be noted in this figure are: (a) the full width at half maximum (FWHM) normalized radius r/R_0 of the Gaussian density radial distribution, in the limit of no-rotation ($\omega_i = 0$), decreases with increasing $\Delta\phi$; (b) the ion angular rotation frequencies (ω_i) increase with $\Delta\phi$ and with the FWHM normalized radius; (c) the permissible range of ion angular rotation frequencies (under equilibrium) considering a FWHM normalized radius between, say, 0.2 and 0.3, for each value of $\Delta\phi$, decreases sharply with increasing $\Delta\phi$. Although $\Delta\phi$ has been specified between r = 0 and $r = R_0 = 10$cm, for purposes of comparison with experimental results the electric potential difference to be considered should be taken between the column axis (r = 0) and the radial distance in which the plasma density is still significant, i.e., just before the plasma sheath region where the plasma neutrality condition may not be satisfied.

The radial number density distribution of the lightest ion (Ni) is not shown here. However, the radial dependence of the separation factor $\alpha_0(r)$, which gives the ratio of the two ion species number densities, according to (61), is presented in Fig. 4, with the ion rotation frequency ω_i (in units of 10^4Hz) as parameter. It must be noted that $\alpha_0(r)$ increases sharply with increasing ω_i and r. The electron number density $n_e(r)$ is given by the sum of the ion number densities at each radial position, according to (18).

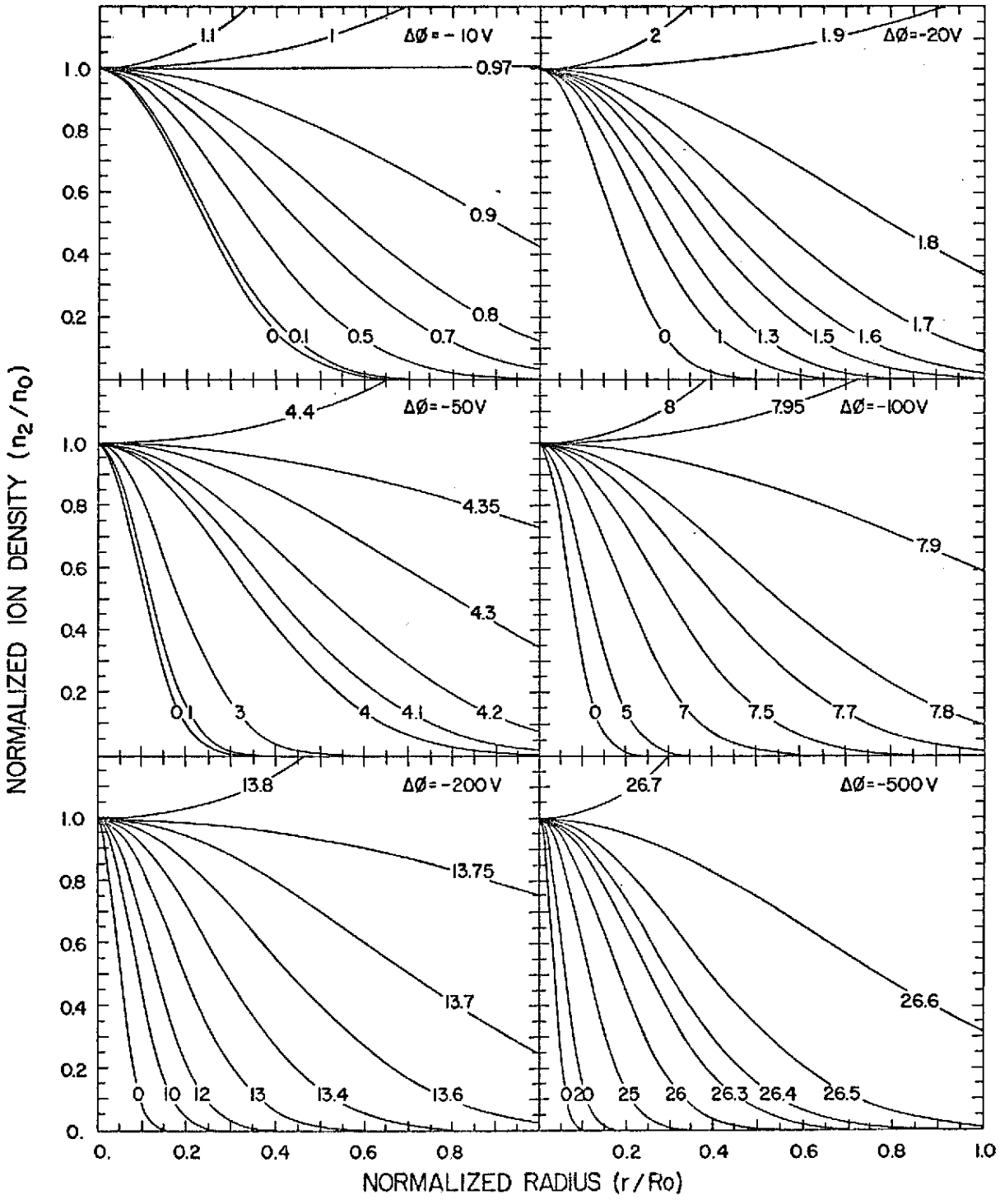

Fig. 3 - Radial number density distribution of the heaviest ion (Cu) for various values of the electric potential difference $\Delta\phi$ between the column axis and the R_0 = 10cm radial distance, with the ion rotation frequency ω_i (in units of 10^4Hz) as parameter, for B = 0.2T and Z_i = 1.

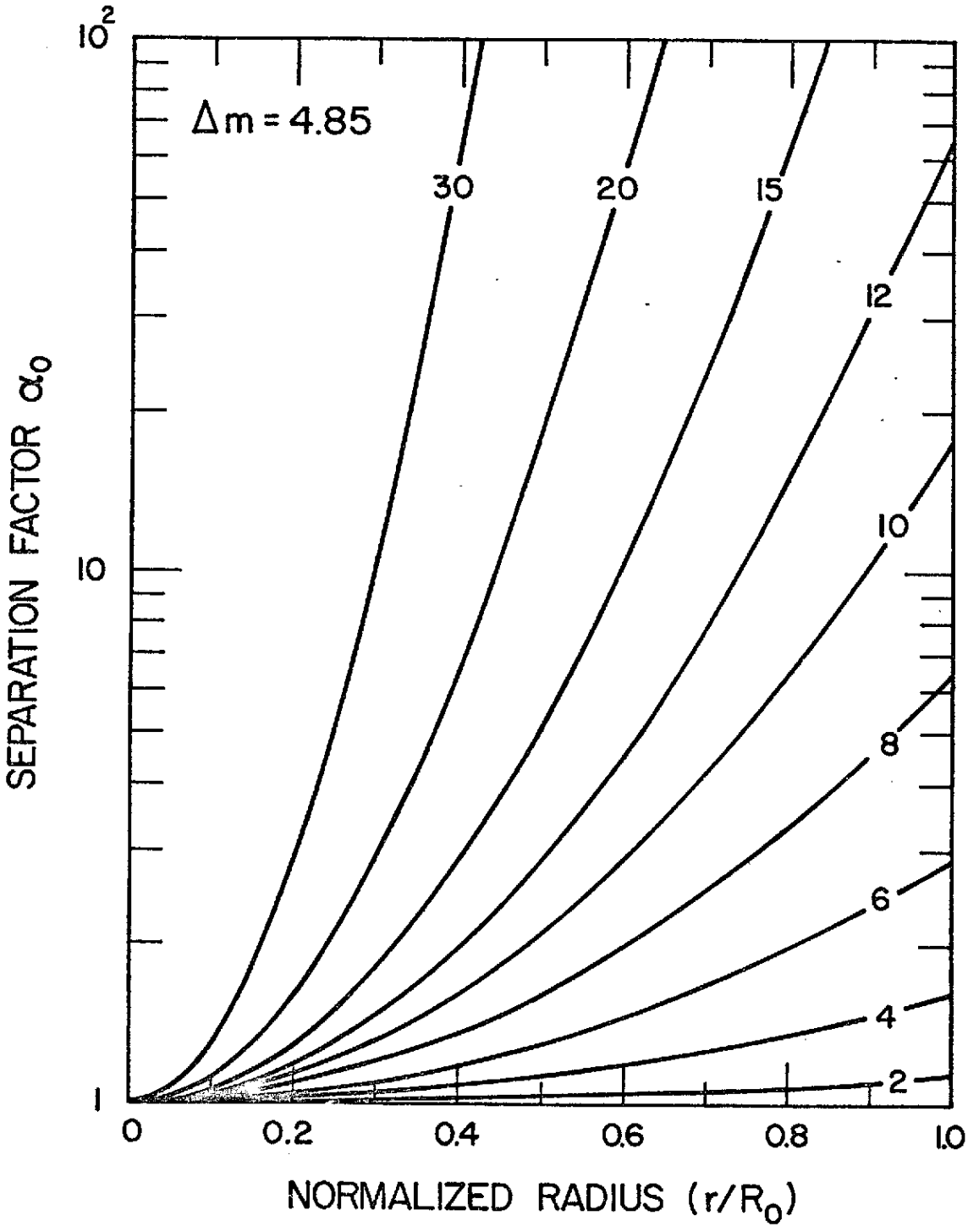

Fig. 4 - Radial dependence of the separation factor α_0 for the Ni-Cu plasma mixture (for which Δm = 4.85amu), with the ion rotation frequency ω_i (in units of 10^4Hz) as parameter.

Plots similar to the one presented in Fig. 3 are shown in Figs. 5 and 6, in which B = 0.2T, Z_i = 3 and B = 1.0T, Z_i = 3, respectively. Comparing with Fig. 3, it is seen that the increase in the value of Z_i (Fig. 5) reduces the FWHM normalized radius r/R_0 in the limit of no-rotation and increases slightly the ion angular rotation frequency, for a given $\Delta\phi$, the effect being more pronounced for larger values of $\Delta\phi$. A comparison between Figs. 6 and 5 shows that the ion angular rotation frequency decreases sharply with increasing magnetic field, for a given $\Delta\phi$, whereas the FWHM normalized radius r/R_0 in the no-rotation limit does not change, as it depends only on the pressure gradient and the radial dependence of the electrostatic potential. It should be noted that this result does not necessarily mean, in a practical situation, that ω_i decreases as B is increased, since experimentally (Geva et al., 1984) it is observed that $\Delta\phi$ varies with B and depends also on other parameters such as the geometry and nature of the produced plasma. Therefore, the dependence of $\Delta\phi$ on B should be determined experimentally for each type of plasma being analyzed, in order to select the B value which maximizes the ion angular rotation frequency.

It is important to compare the ion angular rotation frequencies presented in Figs. 3, 5 and 6, for steady state conditions, with the corresponding ion cyclotron frequencies, $Z_i eB/m_i$, and electromagnetic $\vec{E} \times \vec{B}$ angular rotation frequencies, $|E_r|/rB$. Fig. 7 shows the ion cyclotron frequency Ω_{ci} as a function of B for both Ni and Cu and for Z_i = 1 and Z_i = 3, whereas Fig. 8 presents the electromagnetic $\vec{E} \times \vec{B}$ angular rotation frequency as a function of $\Delta\phi$ for several values of B as parameter. For most cases ω_i is usually less than Ω_{ci}, but it may exceed Ω_{ci} for sufficiently large values of $\Delta\phi$, since ω_i increases with $\Delta\phi$ for a given B field and FWHM normalized radius. On the other hand, considering a negative radial pressure gradient (confined plasma), it is seen that ω_i is always smaller than $|E_r|/rB$. This is due to the fact that the diamagnetic drift is in opposite directions for charges of opposite sign, so that it adds to the electromagnetic drift for the electrons and substracts to the electromagnetic drift for the ions (for a negative radial pressure gradient).

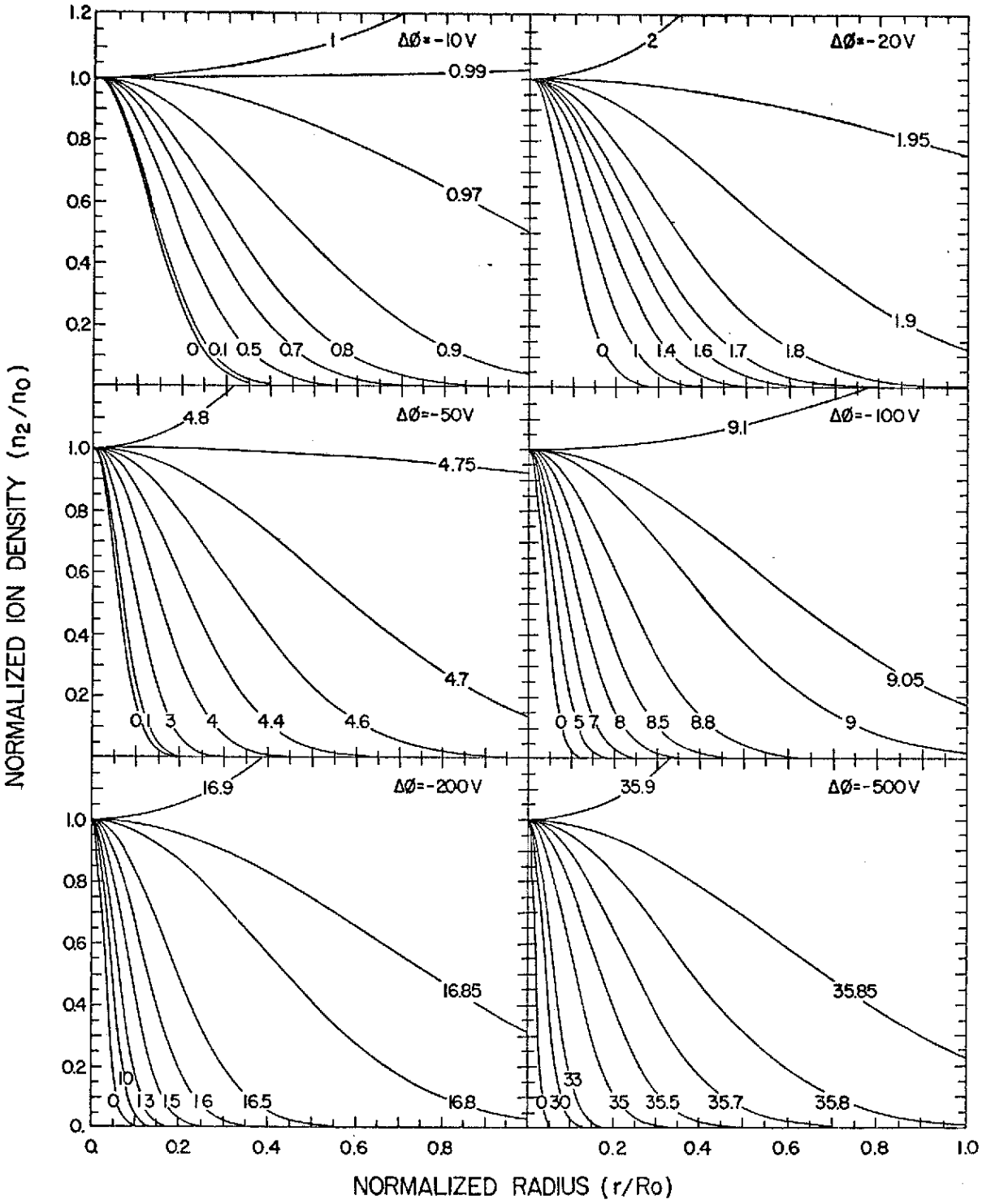

Fig. 5 - Same as in Fig. 3, but for B = 0.2T and Z_i = 3.

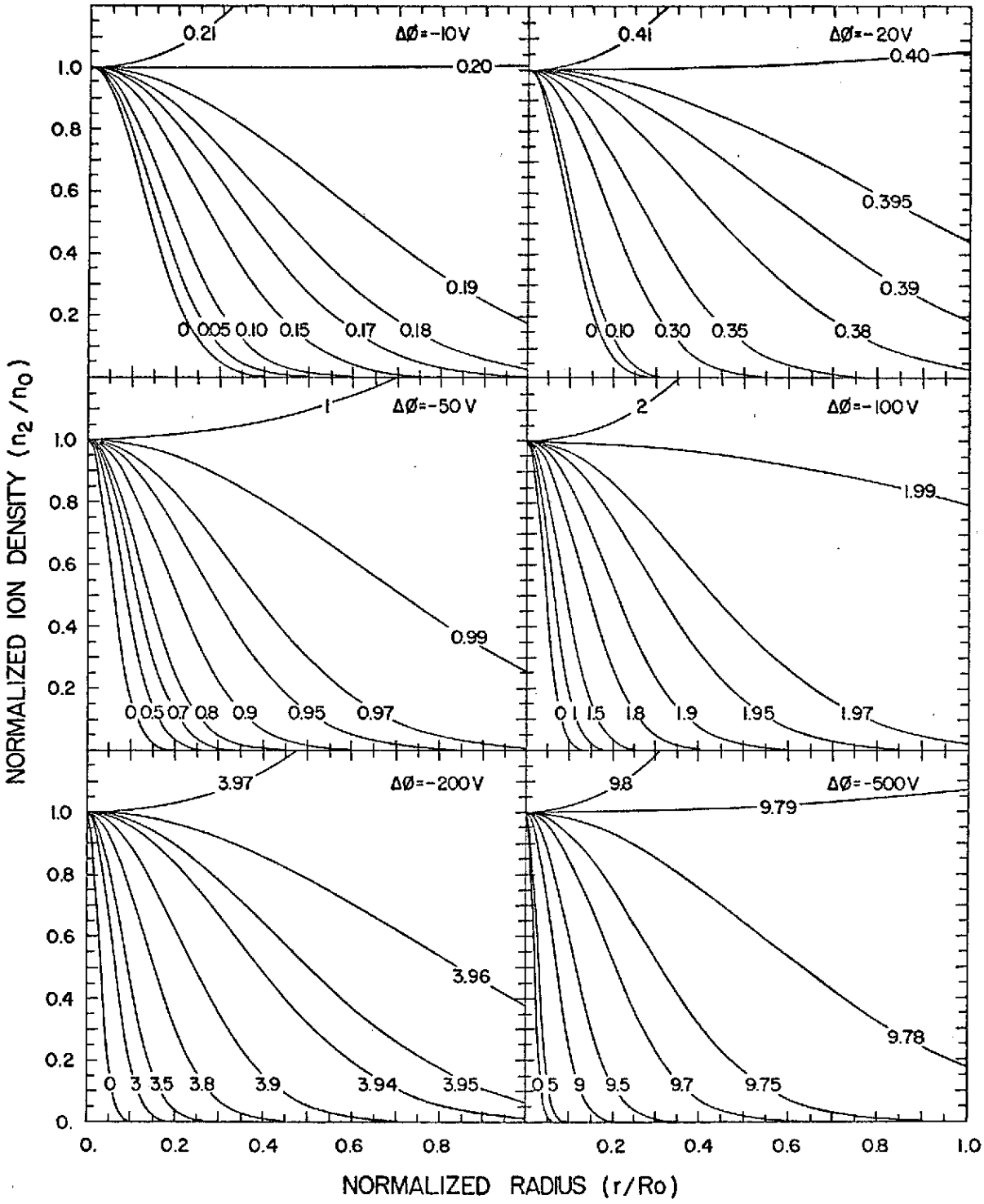

Fig. 6 - Same as in Fig. 3, but for B = 1.0T and Z_i = 3.

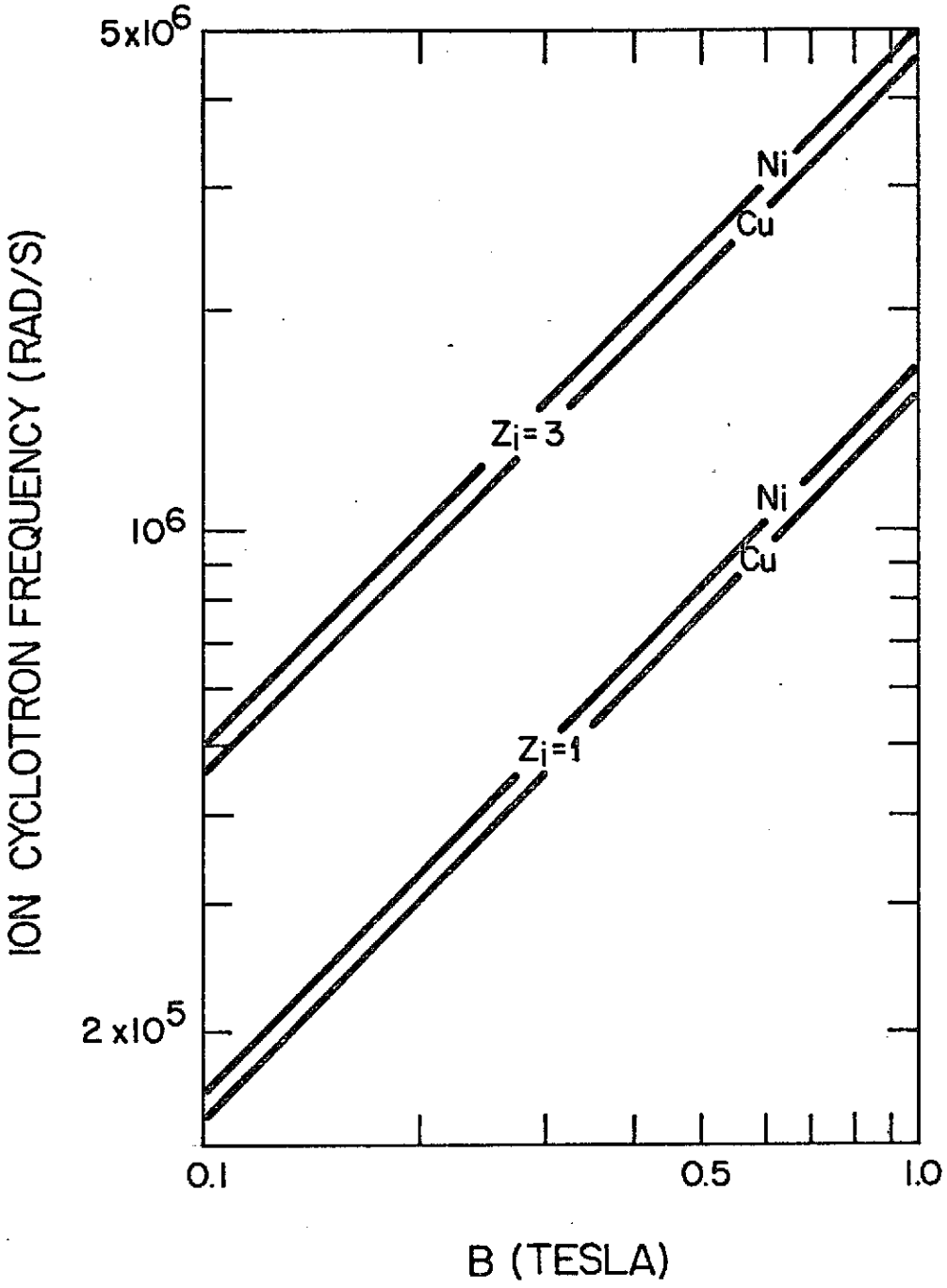

Fig. 7 - Ion cyclotron frequency Ω_{ci} for Ni and Cu, as a function of the magnetic induction B, considering $Z_i = 1$ and $Z_i = 3$.

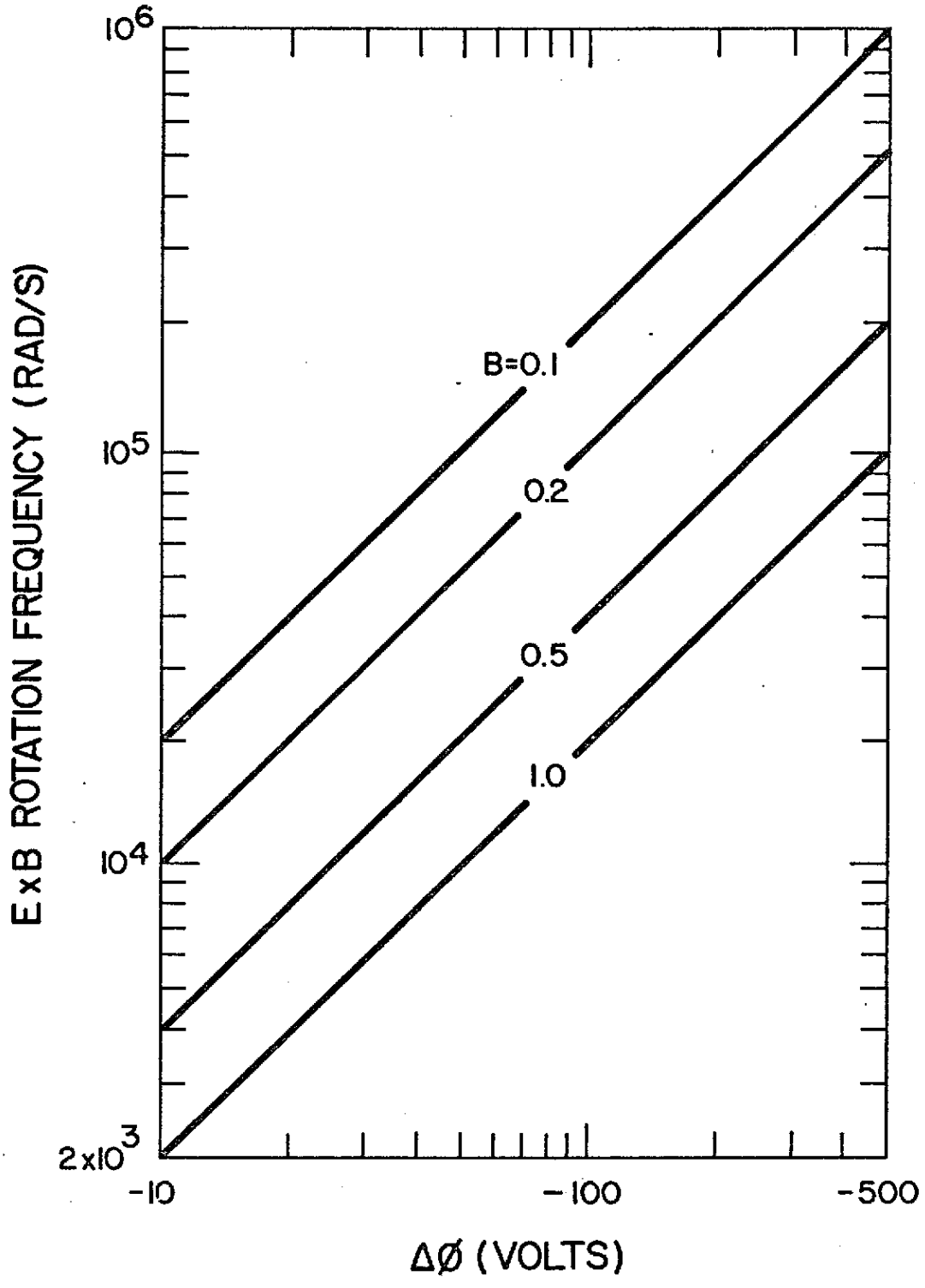

Fig. 8 - Electromagnetic $\vec{E} \times \vec{B}$ angular rotation frequency (E_r/rB) as a function of the electric potential difference $\Delta\phi$ between the column axis and the R_0 = 10cm radial distance, with the magnetic induction B as parameter.

For $\omega_i = |E_r|/rB$ the radial ion pressure gradient must be positive. However, for values of the FWHM normalized radius greater than, say, 0.2 and for relatively large values of $\Delta\phi$, the effect of the diamagnetic drift becomes small, so that ω_i may get very close to the electromagnetic drift, i.e.,

$$\omega_i \lesssim |E_r|/rB \ . \tag{67}$$

The confinement of the plasma is due to the resulting $\vec{J}_\theta \times \vec{B}$ radial force density, which is radially inward for $J_\theta < 0$ (i.e., $u_{e\theta} > u_{i\theta}$). The radial distribution of the azimuthal current density is illustrated in Fig. 9, considering $\Delta\phi = -10V$ and $\Delta\phi = -100V$, with ω_i (in units of 10^4Hz) as parameter, for the case in which $B = 0.2T$ and $Z_i = 3$, calculated from the expression

$$J_\theta(r) = \sum_\alpha q_\alpha n_\alpha(r) u_{\alpha\theta}(r) \ ,$$

$$= er[Z_1\omega_1 n_1(r) + Z_2\omega_2 n_2(r) - \omega_e n_e(r)] \ . \tag{68}$$

The dashed line indicates that the current has reversed direction, so that J_θ is negative for $\omega_e > \omega_i$ (full lines) and is positive for $\omega_e < \omega_i$ (dashed line). The azimuthal current falls abruptly to zero when $\omega_e = \omega_i$.

The results shown in Figs. 3, 5 and 6 can be presented in a more compact manner without showing the radial dependence of $n_i(r)$. The quantities involved are ω_i, $\Delta\phi$ and the FWHM normalized radius for $n_2(r)$, where the radial dependences are linear for $u_i(r)$, parabolic for $\phi(r)$ and Gaussian for $n_i(r)$. Thus, Fig. 10 shows ω_i versus $\Delta\phi$, with the FWHM normalized radius as parameter, corresponding to the results presented in Fig. 3, for $B = 0.2T$ and $Z_i = 1$. The most important feature of these results is the sharp decrease in the range of allowed equilibrium values of ω_i, as $\Delta\phi$ increases, considering a given range of values for the FWHM normalized radius.

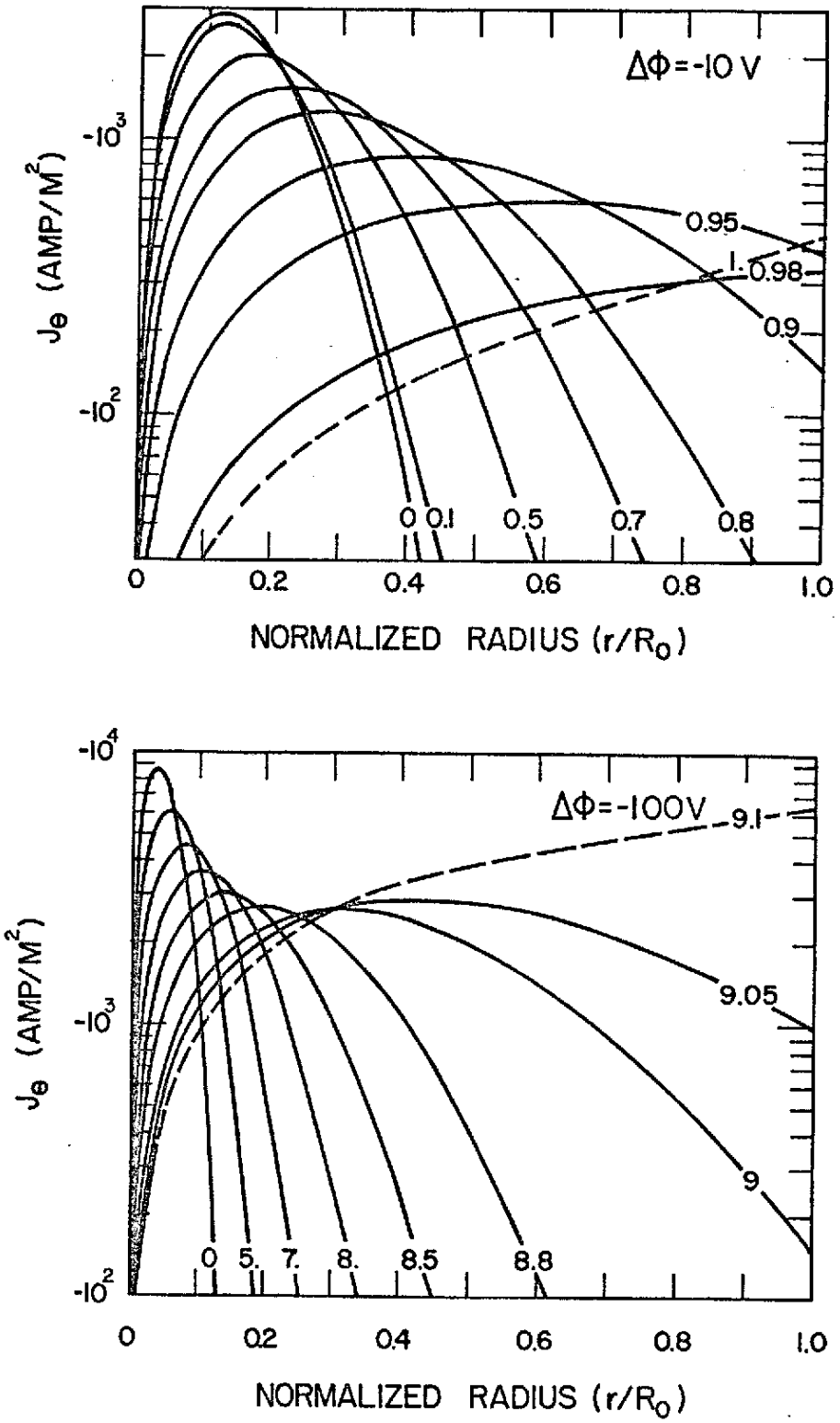

Fig. 9 - Radial distribution of the azimuthal current density $J_\theta(r)$, with the ion rotation frequency ω_i (in units of 10^4Hz) as parameter, considering $\Delta\phi$ = -10V and $\Delta\phi$ = -100V, for B = 0.2T and Z_i = 3.

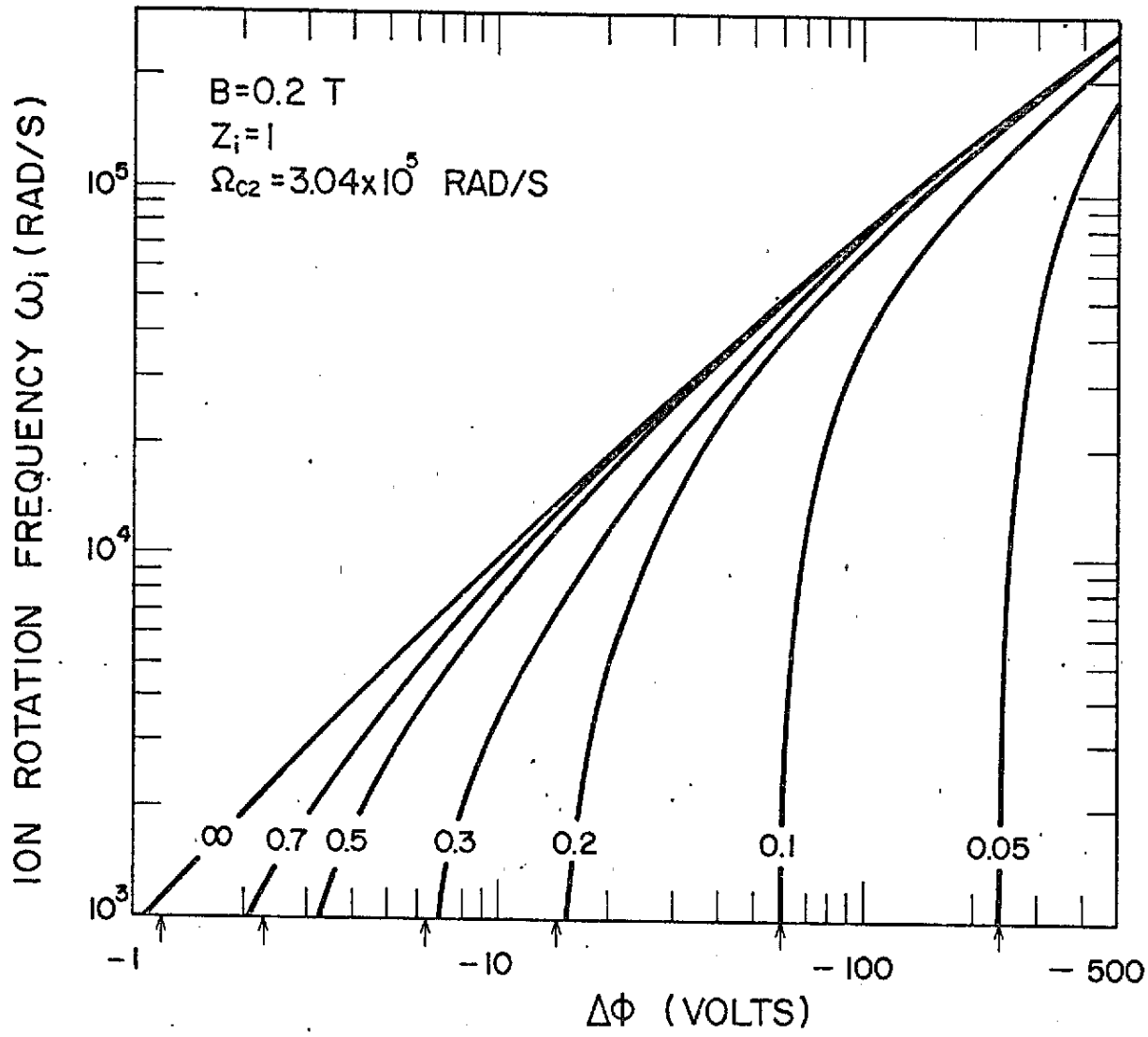

Fig. 10 - Ion rotation frequency ω_i as a function of the electric potential difference $\Delta\phi$ between the column axis and the R_0 = 10cm radial distance, with the full width at half maximum (FWHM) normalized radius r/R_0 as parameter, for B = 0.2T and Z_i = 1.

The arrows along the abscissa indicate the corresponding asymptotic value for each parametric curve. These same results are plotted in a different manner in Figs. 11 and 12, for purposes of illustration, where it is shown ω_i versus the FWHM normalized radius with $\Delta\phi$ as parameter (Fig. 11), and the FWHM normalized radius versus $\Delta\phi$, with ω_i as parameter (Fig. 12). Thus, choosing any reasonable values for two of these parameters, the other one is uniquely determined according to the steady state equation of motion (36). Alternatively, fixing one of these parameters, its corresponding parametric curve indicates how the other two parameters must vary according to equilibrium conditions.

Another variable which is uniquely determined once any two of the parameters ω_i, $\Delta\phi$ and FWHM are kept fixed, is the electron angular rotation frequency ω_e, as can be seen from (35), since $n_e(r)$ is determined by charge neutrality. For illustration purposes, it is presented in Fig. 13 the FWHM normalized radius for $n_2(r)$ (full lines) and the electron angular rotation frequency ω_e (dashed lines) as a function of $\Delta\phi$, in the limit of no ion rotation ($\omega_i = 0$), for several values of B and Z_i as parameters. Note that the lines for the FWHM are independent of B, as discussed previously with reference to Figs. 5 and 6. It is seen that the FWHM normalized radius decreases with $\Delta\phi$, as illustrated in Figs. 3, 5 and 6, whereas ω_e increases with $\Delta\phi$, but decreases with B. Also, the FWHM decreases as ω_e increases, since for $\omega_i = 0$ the radial confining force density on the plasma is provided by the azimuthal electron current density.

Four principal variables are therefore involved in order to picture the steady state behavior of the rotating plasma column, which are ω_i, ω_e, $\Delta\phi$ and the FWHM normalized radius for $n_2(r)$. The relationship between these four variables under equilibrium conditions is illustrated in Fig. 14, where it is shown ω_i as a function of ω_e, with both $\Delta\phi$ and the FWHM normalized radius as parameter, for the case in which B = 0.2T and $Z_i = 1$. The arrows along the abscissa indicate the asymptotic values corresponding to each parametric curve for $\Delta\phi$. The dashed straight line is the 45^o slope line, for which $\omega_i = \omega_e$.

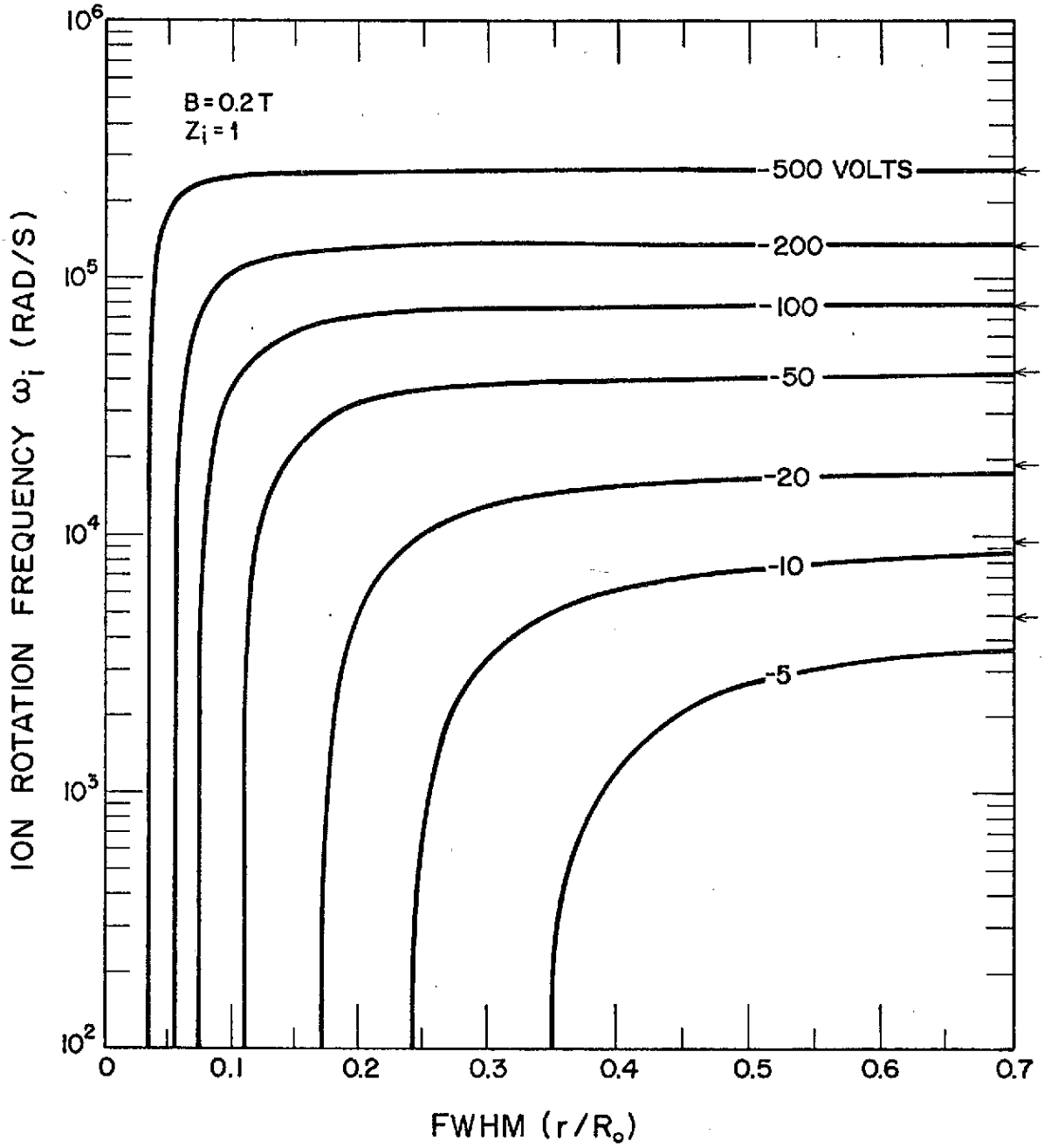

Fig. 11 - Ion rotation frequency ω_i as a function of the full width at half maximum (FWHM) normalized radius r/R_0, having as parameter the electric potential difference $\Delta\phi$ between the column axis and the $R_0 = 10$cm radial distance, for $B = 0.2$T and $Z_i = 1$.

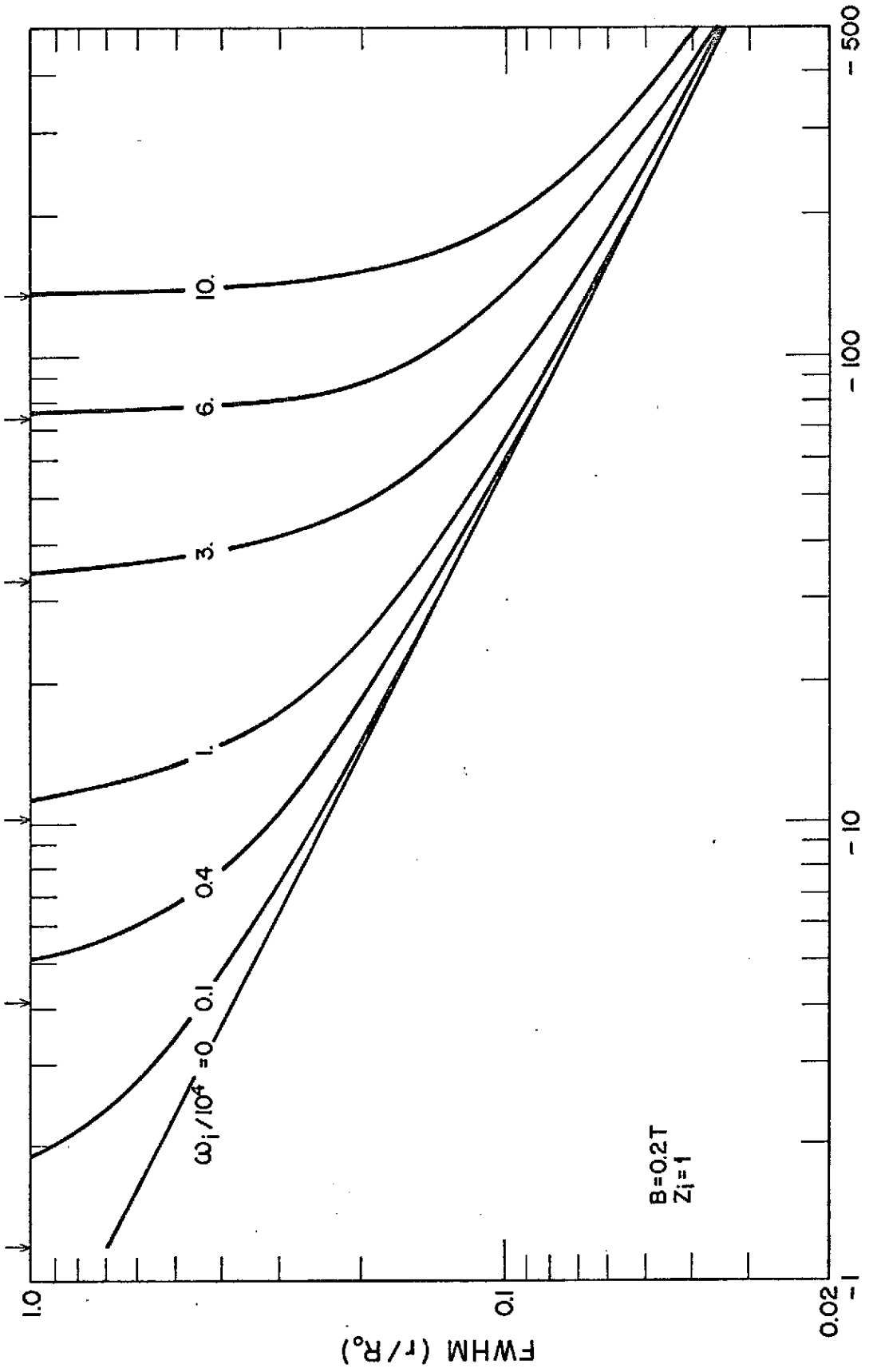

Fig. 12 - Full width at half maximum (FWHM) normalized radius r/R_0 as a function of the electric potential difference $\Delta\phi$ between the column axis and the $R_0 = 10$cm radial distance, with the ion rotation frequency ω_i (in units of 10^4Hz) as parameter, for B=0.2T and $Z_i = 1$.

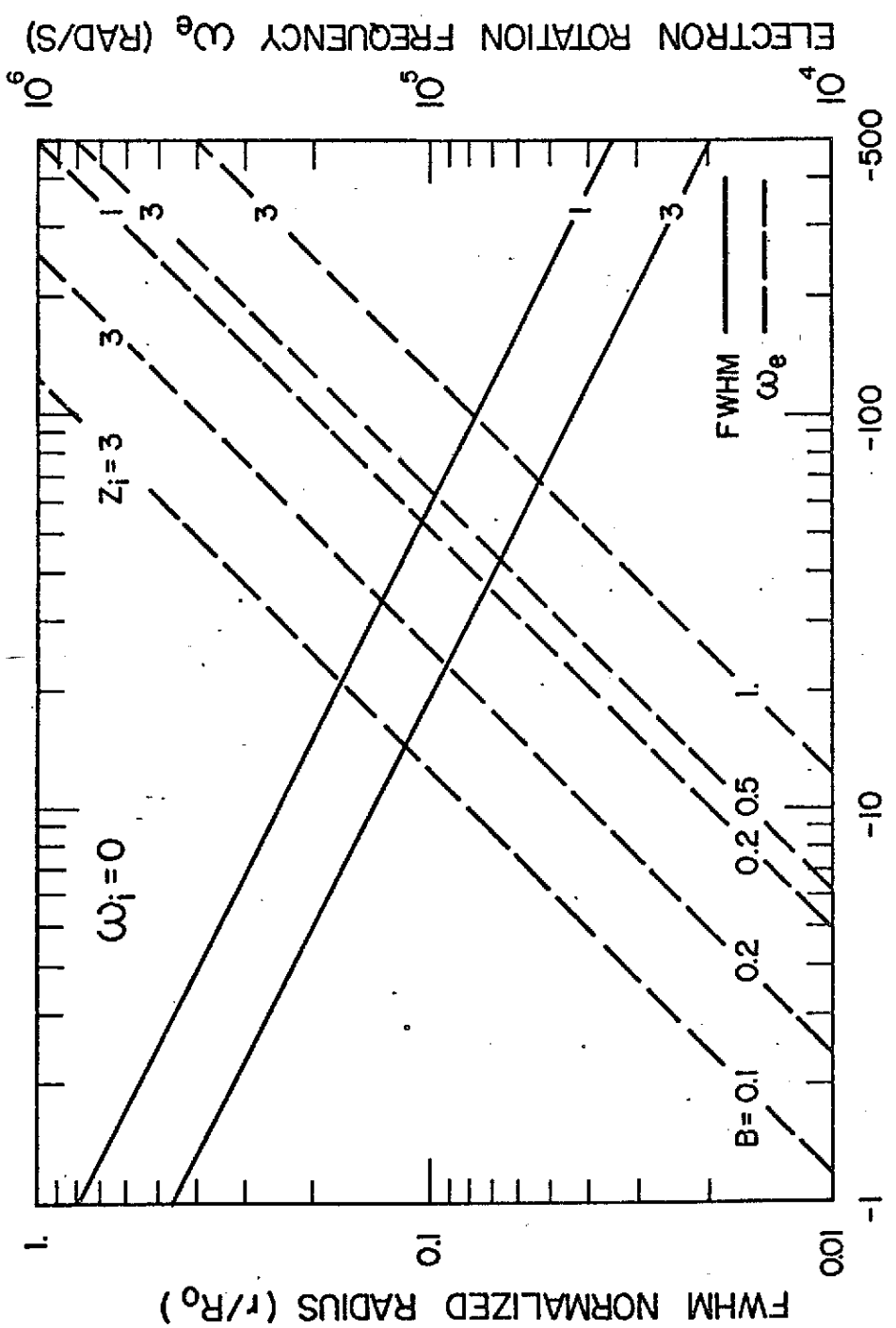

Fig. 13 - Full width at half maximum (FWHM) normalized radius r/R_0 (full lines) and electron rotation frequency ω_e (dashed lines) as a function of the electric potential difference $\Delta\phi$ between the column axis and the R_0 = 10cm radial distance, in the limit of no ion rotation (ω_i = = 0), with the magnetic induction B and the ionization state Z_i as parameters.

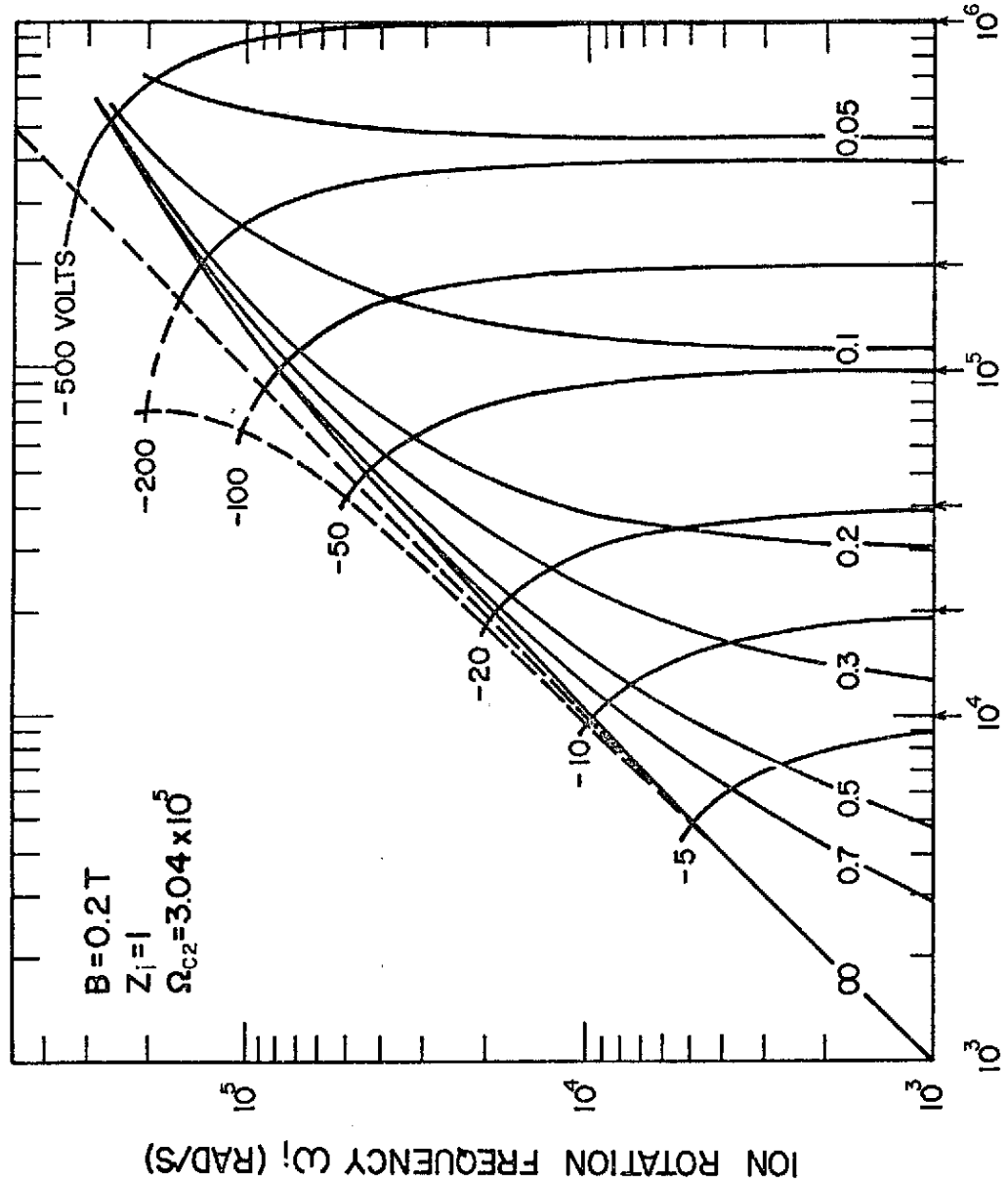

Fig. 14 - Ion rotation frequency ω_i as a function of the electron rotation frequency ω_e, having as parameters the full width at half maximum (FWHM) normalized radius r/R_0 and the electric potential difference $\Delta\phi$ between the column axis and the R_0=10cm radial distance, for B=0.2T and Z_i=1.

The dashed curve in the region where $\omega_i > \omega_e$ indicates the situation in which $\omega_i = |E_r|/rB$. Note that, since $m_2 > m_1$ (where the indices 1 and 2 denote Ni and Cu, respectively), when the conditions are such that the FWHM for n_2 tends to infinity (constant density for copper), the radial distribution of the Ni number density still shows a negative radial pressure gradient. For a higher value of ω_i such that n_1 becomes constant with radius, n_2 will already show a positive radial pressure gradient. The allowed values of the various variables for a confined plasma are located in the region where $\omega_e > \omega_i$. Experimentally observed values of the FWHM normalized radius are around 0.25 (Geva et al., 1984), so that the FWHM parametric curves labeled 0.2 and 0.3 presumably limitate the region where the experimentally observed points should be located, under equilibrium conditions. For relatively large values of $\Delta\phi$ this region becomes extremelly small.

A similar plot is shown in Fig. 15 for the case in which $B = 0.2T$ and $Z_i = 3$. Higher ion angular rotation frequencies are obtained in Fig. 15, for the same values of $\Delta\phi$ and FWHM. For example, considering $\Delta\phi = -100V$ and a FWHM normalized radius of 0.25, Fig. 14 yields $\omega_i \cong 7 \times 10^4$rad/s, whereas Fig. 15 yields $\omega_i \cong 9 \times 10^4$rad/s. In both cases $\omega_e > 10^5$rad/s. In order to show the dependence of the various equilibrium variables on the magnetic field, similar results are presented in Figs. 16, 17 and 18 for the cases in which $B = 0.1T$, $B = 0.5T$ and $B = 1.0T$, respectively, with $Z_i = 3$. It is seen that smaller ion angular rotation frequencies are obtained as B increases, for the same values of $\Delta\phi$ and FWHM. For example, considering $\Delta\phi = -100V$ and a FWHM normalized radius of 0.25, it is obtained $\omega_i \cong 1.5 \times 10^5$rad/s for $B = 0.1T$ (Fig. 16) and $\omega_i \cong 2 \times 10^4$rad/s for $B = 1.0T$ (Fig. 18).

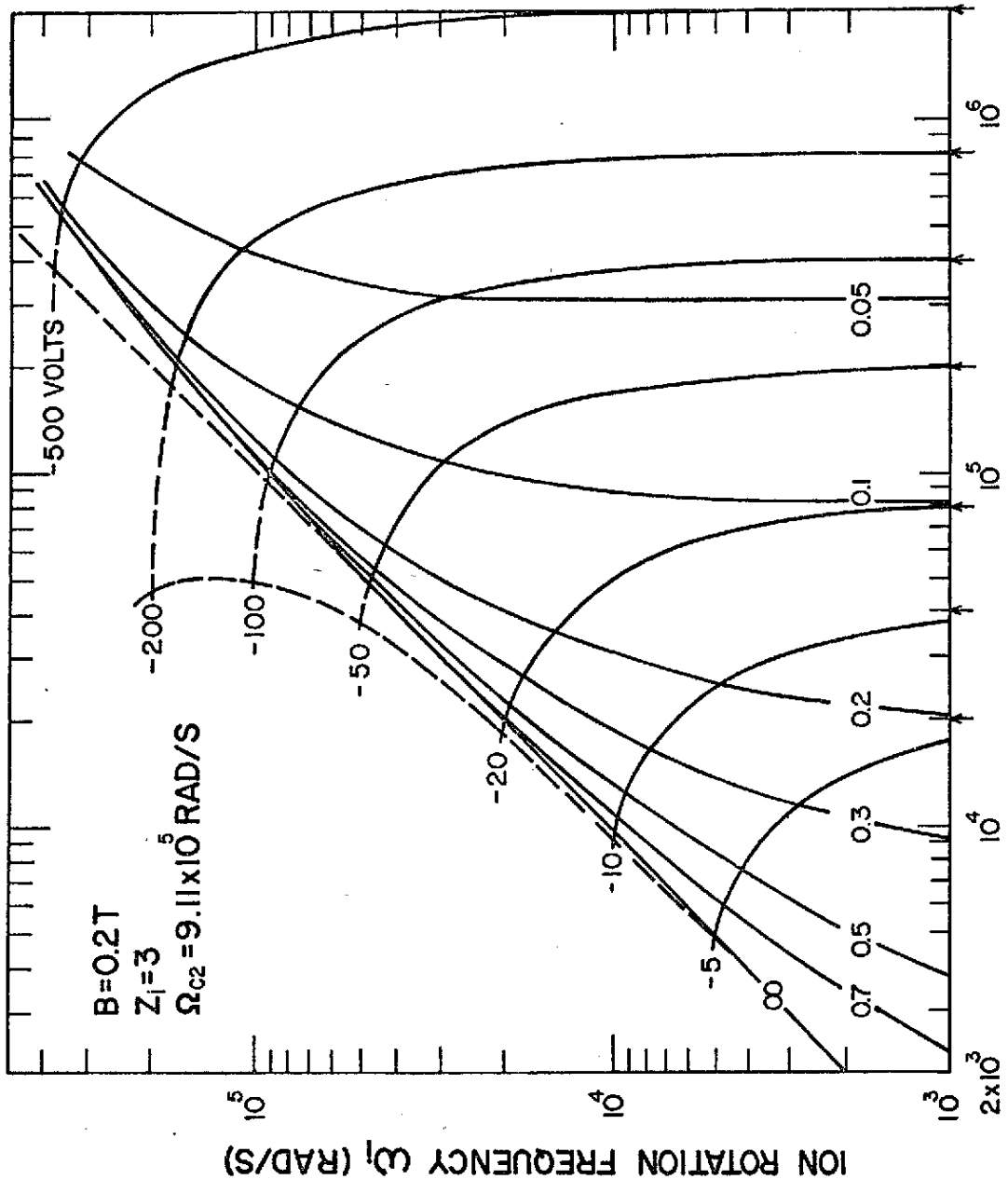

Fig. 15 - Same as in Fig. 14, but for B = 0.2T and Z_i = 3.

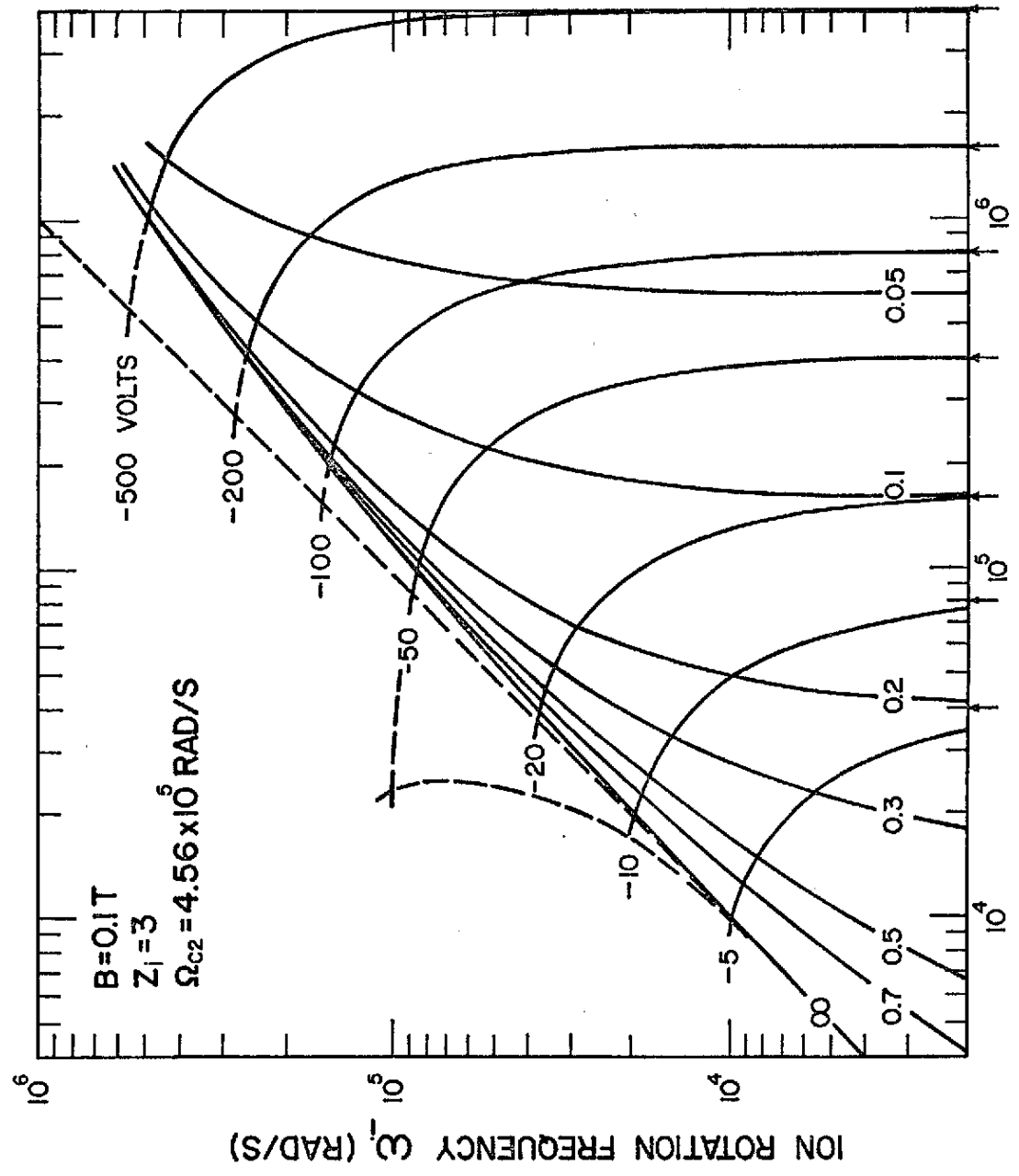

Fig. 16 - Same as in Fig. 14, but for B = 0.1T and Z_i = 3.

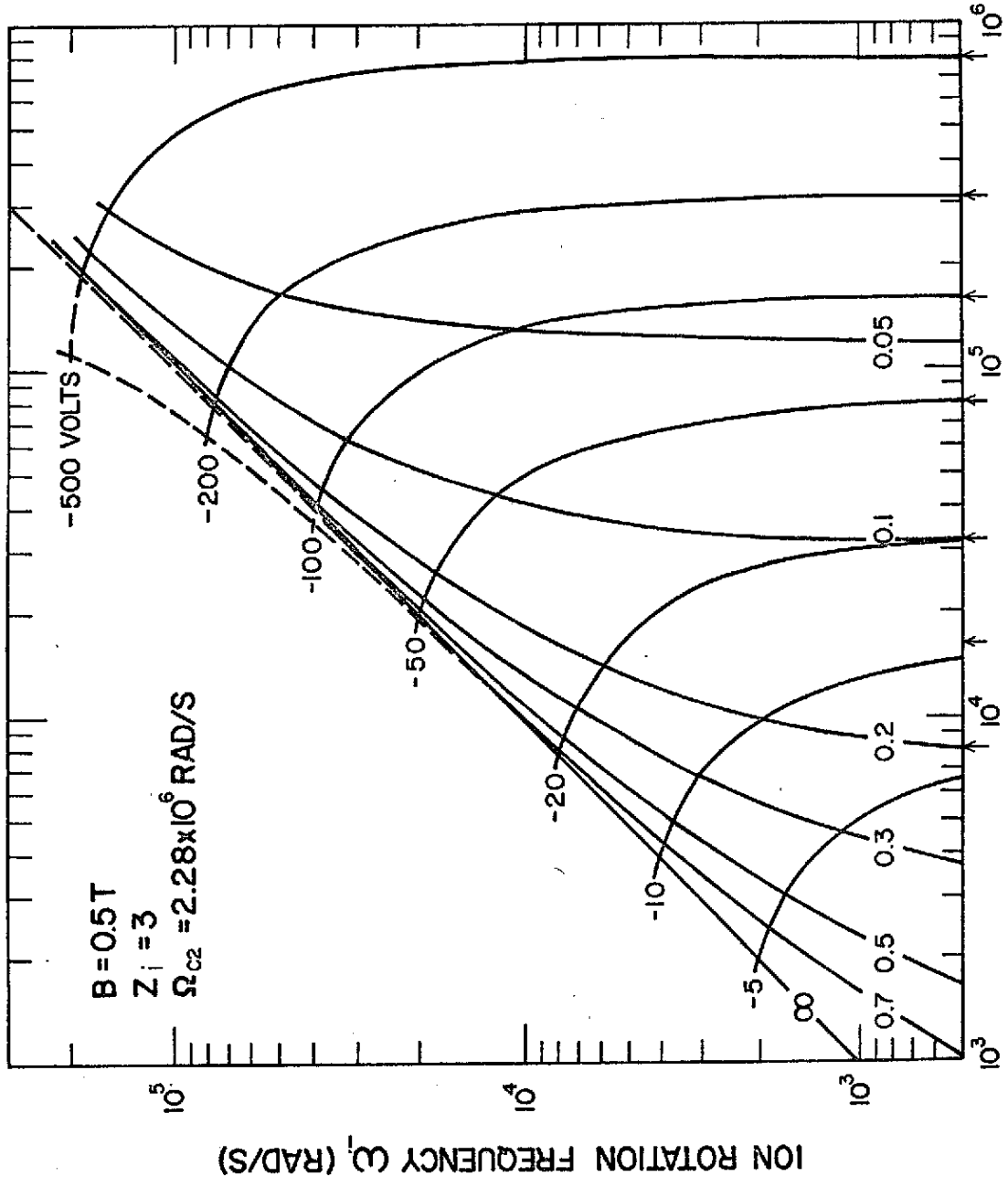

Fig. 17 - Same as in Fig. 14, but for B = 0.5T and Z_i = 3.

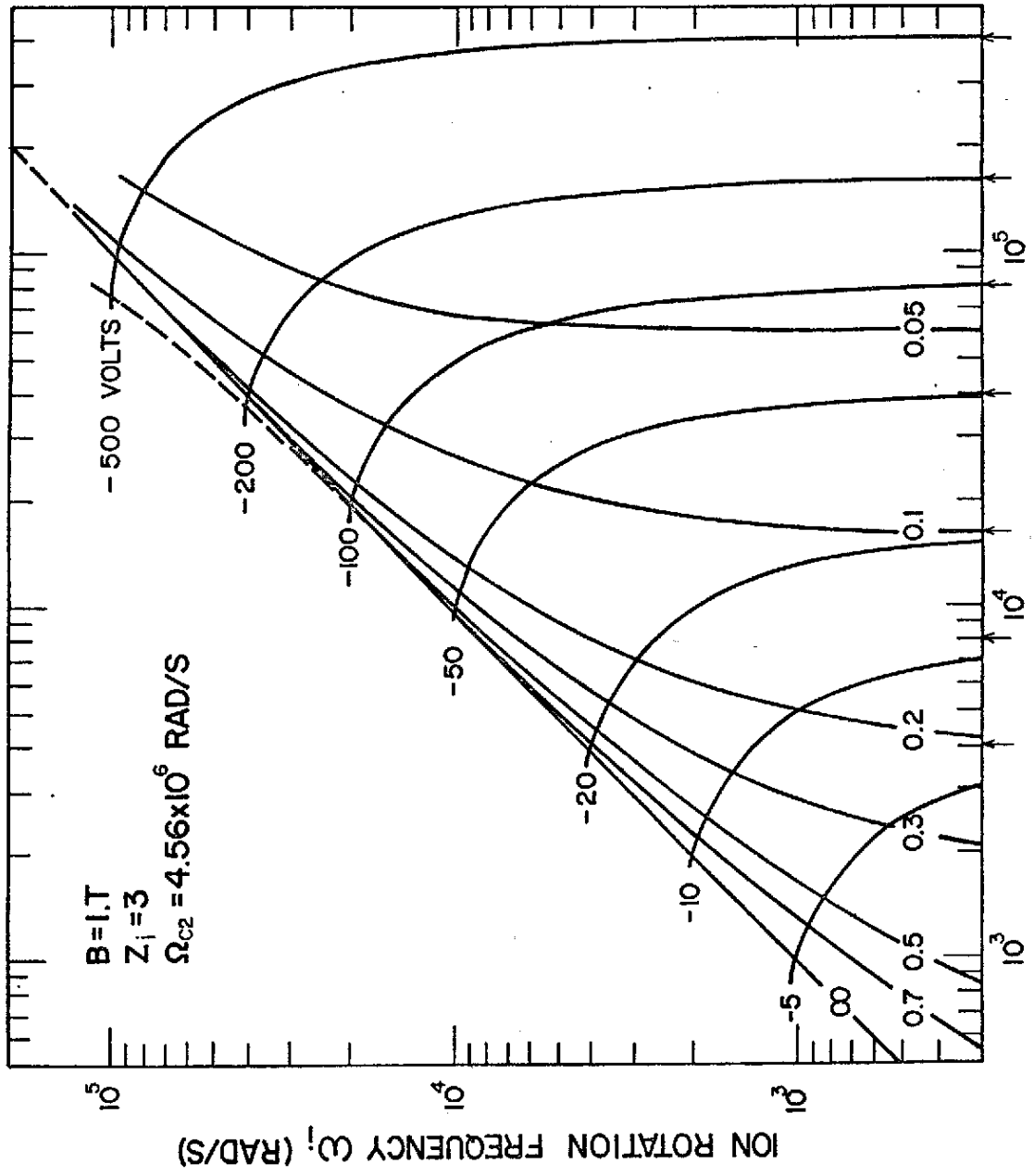

Fig. 18 - Same as in Fig. 14, but for B = 1.0T and Z_i = 3.

Measurements made by Geva et al. (1984) for a Ni-Cu plasma at about 90cm downstream from the cathode showed a Gaussian radial ion density distribution with a FWHM radius of 2.5cm, a parabolic radial dependence for the electric potential inside the plasma with a potential drop of about 8V between $r = 0$ and $r = 3cm$ (which extrapolates to $\Delta\phi = 89V$ at $r = 10cm$) and an ion angular rotation frequency $\omega_i = 7.9 \times 10^4 rad/s$, for $B = 0.13T$ and $\langle Z_i \rangle = 3$ (Fig. 11 of Geva et al., 1984). These experimental results are in good agreement with the theoretical predictions for steady state equilibrium conditions, presented in Figs. 15 and 16, calculated for $B = 0.2T$ and $B = 0.1T$, respectively, considering the uncertainties and approximations involved.

Fig. 19 illustrates explicitly the dependence of the ion angular rotation frequency on the magnetic field intensity for several values of $\Delta\phi$, considering $Z_i = 3$. The parametric curves indicate the corresponding values of the FWHM normalized radius and the number within parenthesis refers to the limiting value of the FWHM when ω_i goes to zero. Note that the region limited by the lines corresponding to a FWHM normalized radius between 0.2 and 0.3, say, decreases sharply as $\Delta\phi$ increases and tends to become just one single line for sufficiently large values of $\Delta\phi$. Hence, in this case, ω_i is uniquely determined for specified values of B and $\Delta\phi$. It must be stressed that this inverse dependence of ω_i with B is valid for a constant value of $\Delta\phi$. However, as mentioned before, the experimentally observed values of $\Delta\phi$ depend on B as well as on other plasma characteristics, so that the dependence of ω_i on B in a practical situation is not that straigthforward. For each experimental situation a relationship between $\Delta\phi$ and B must be determined first, in order to find how ω_i varies with B (and $\Delta\phi$). This is an important aspect to be investigated for deriving scaling laws for plasma centrifuges, since there must be a certain value of B, for a given plasma, which maximizes ω_i and therefore maximizes the separation factor, according to (62).

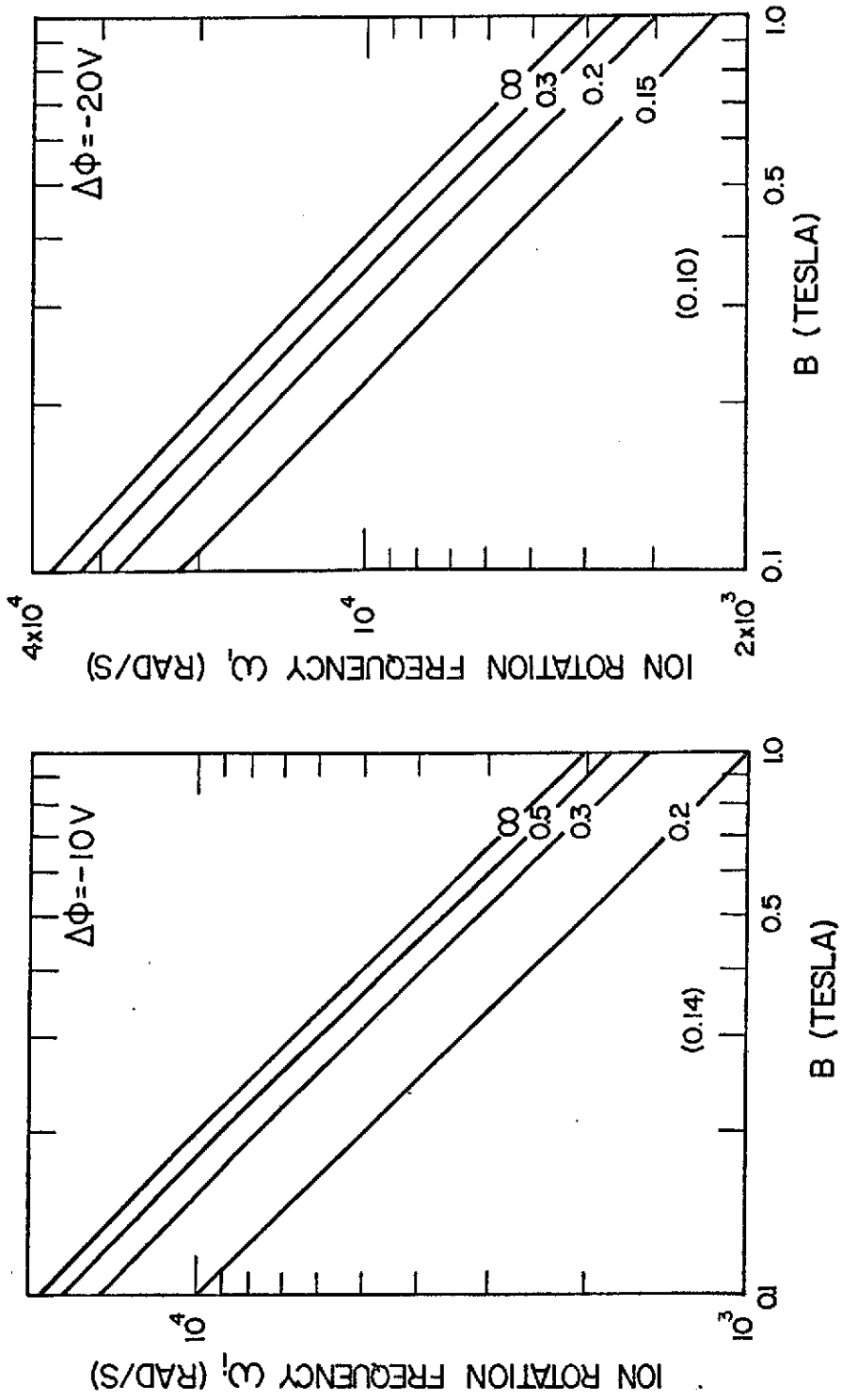

Fig. 19 - Dependence of the ion rotation frequency ω_i on the magnetic induction B, with the full width at half maximum (FWHM) normalized radius r/R_0 as parameter, for various values of the electric potential difference $\Delta\phi$ between the column axis and the $R_0 = 10$cm radial distance.

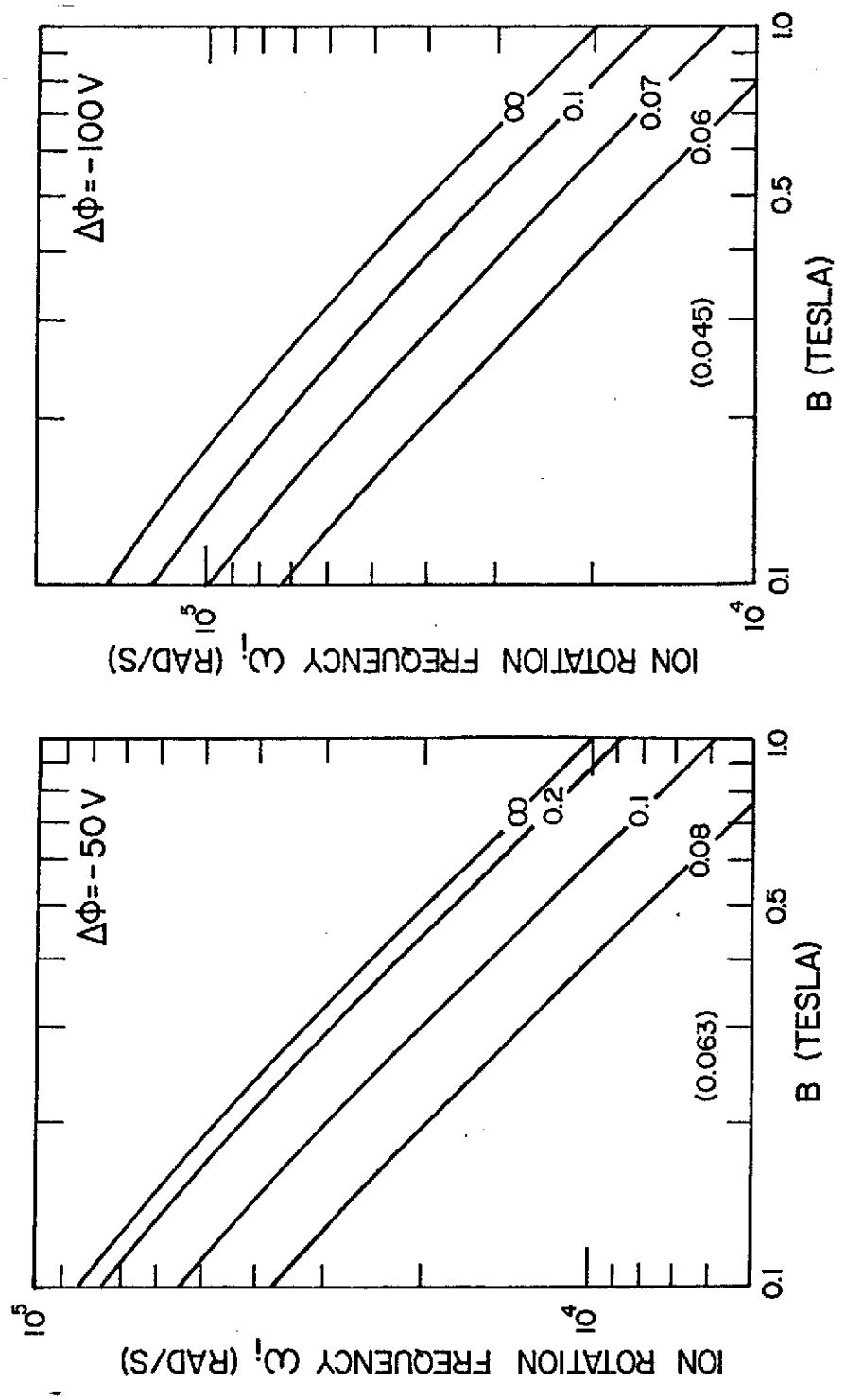

Fig. 19 - (Continued)

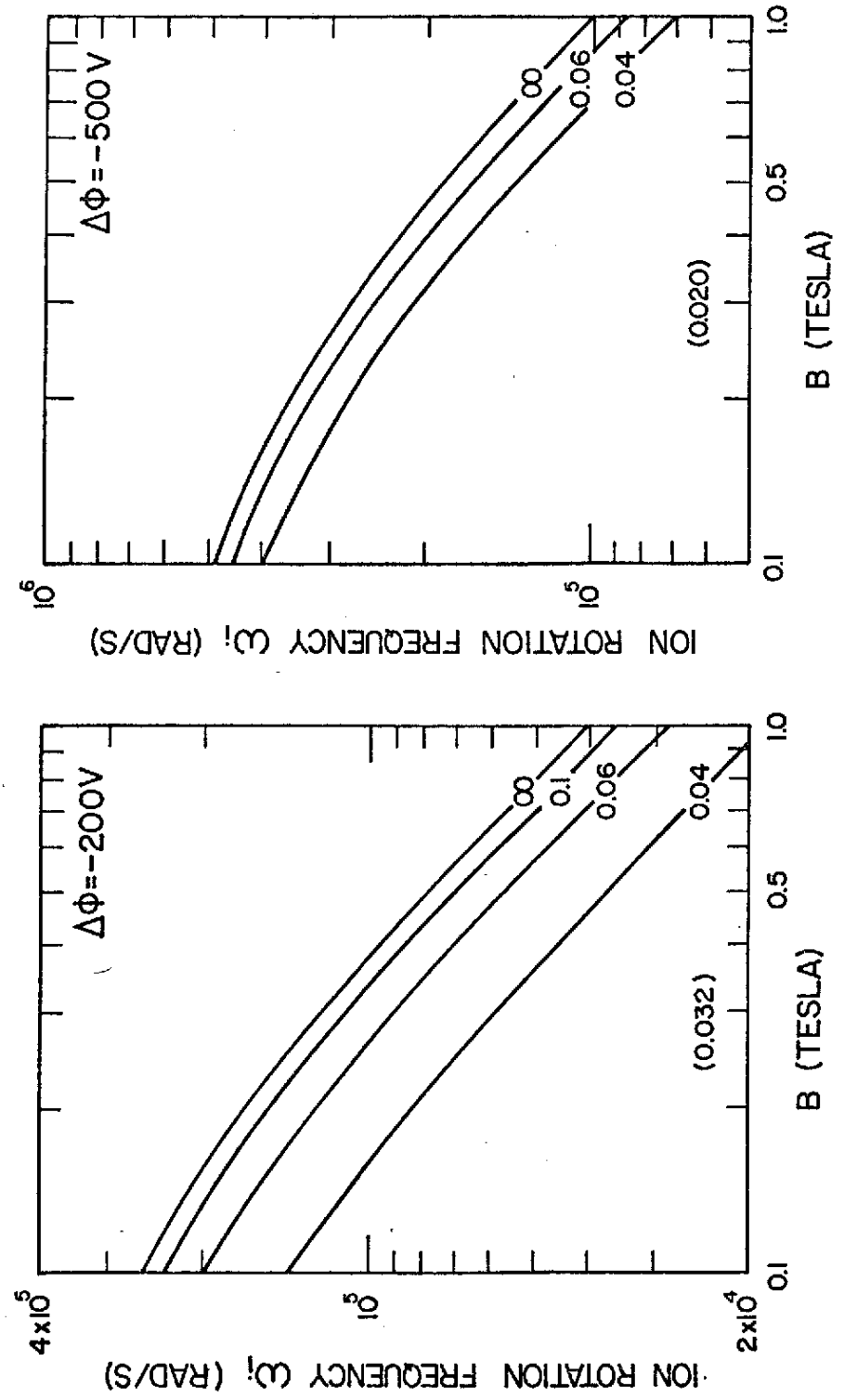

Fig. 19 - (Continued)

Finally, for the purpose of element and isotope separation analysis, onde the ion rotation frequency has been determined, it is shown in Fig. 20 the dependence of the separation factor α_0 on the mass difference m (in atomic mass units) between any two ion species, with ω_i (in units of 10^4Hz) as parameter, at a normalized radial distance $r/R_0 = 0.5$. The importance of achieving large values of ω_i is clearly evident from this plot, if large values of α_0 are to be obtained.

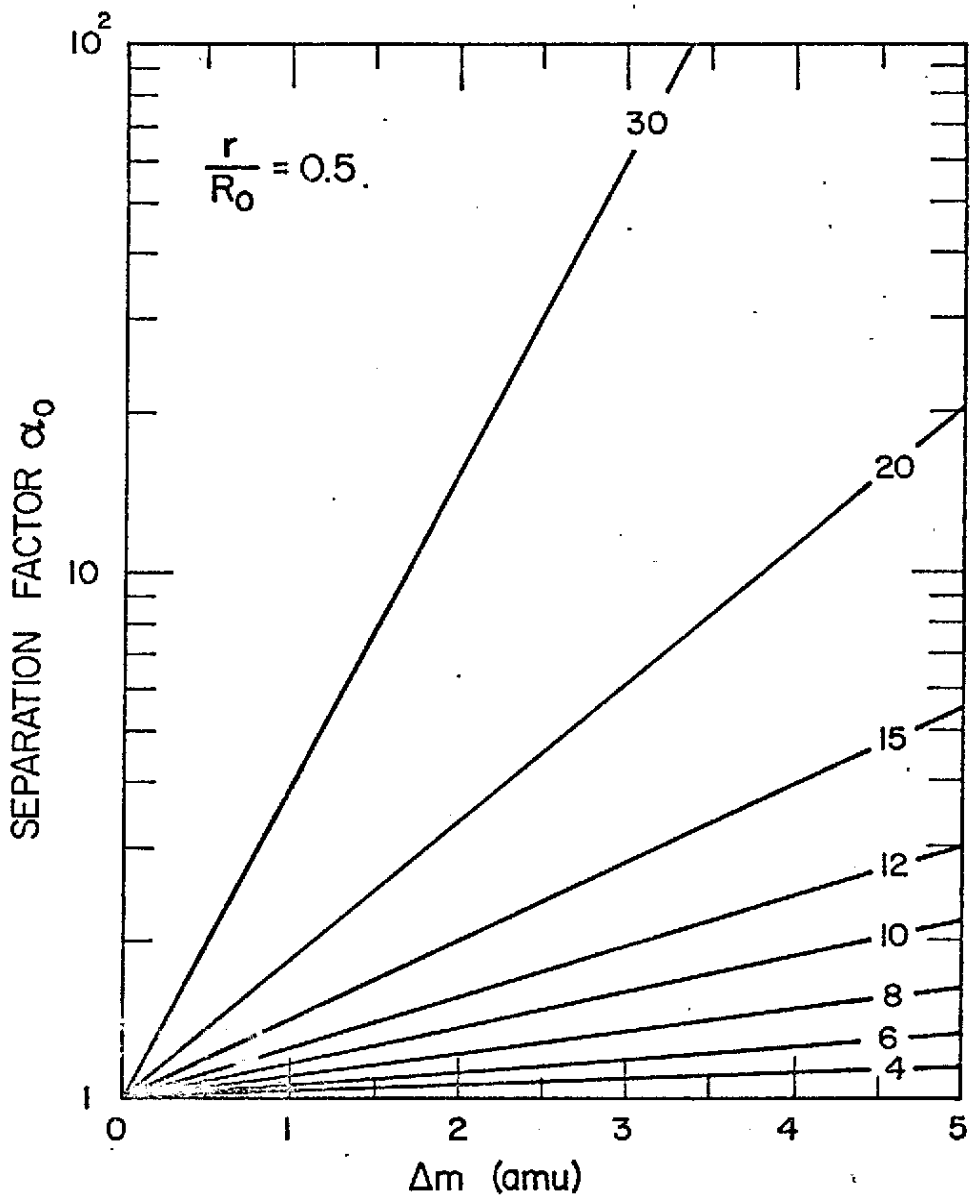

Fig. 20 - Dependende of the separation factor α_0 on the mass difference Δm (in amu) between any two ion species considered, at the radial distance $r/R_0 = 0.5$, with the ion rotation frequency ω_i (in units of 10^4Hz) as parameter.

8. SUMMARY AND CONCLUSIONS

A multiple species fluid model for a fully ionized magnetized plasma under rotation has been described. The model includes electromagnetic, pressure gradient, centrifugal and collisional forces, in cylindrical geometry. A detailed parametric analysis is presented for the steady state behavior of a fully ionized rotating plasma column in a vacuum-arc plasma centrifuge. The parametric dependence of the various plasma parameters, under dynamical equilibrium conditions, is established considering the case of a Ni-Cu plasma. A family of theoretically possible equilibrium configurations is obtained for various combinations of centrifugal, pressure gradient and electromagnetic forces. It is shown that the ion rotation frequency and, therefore, the separation factor increase with the radial electric potential difference (for a given magnetic induction field), but decrease as the magnetic induction increases (for a given radial electric potential difference). The theoretical results show that, essentially, the electron angular rotation frequency is larger than, and the ion angular rotation frequency smaller than the $\vec{E} \times \vec{B}$ angular rotation frequency, the difference being dependent on the FWHM radius of the Gaussian radial density distribution. Since the ion rotation velocity approaches the upper limiting velocity for confinement (which is slightly less than the electromagnetic drift velocity) as the inward radial pressure gradient decreases, it seems convenient to produce a plasma column with a small radial pressure gradient and therefore with a large FWHM radius, in order to achieve higher rotational velocities. This situation also gives a larger plasma density at the outer radii, than oterwise, thus increasing the quantity of enriched plasma. Also, experimental observations have shown that $\Delta\phi(r)$ and B_z depend on one another, and this relationship depends further on the plasma characteristics and geometry. Therefore, it is important to experimentally determine the relationship between $\Delta\phi(r)$ and B_z, for each situation under investigation in a vacuum-arc centrifuge, with

a view to establishing scaling laws for such centrifuges. An appropriate value of B_z can then be selected in order to maximize the ion rotation velocity and the separation factor. The FWHM radius of the ion density radial distribution is another factor which plays a role in the ion rotation velocity and it seems that the cathode geometry and the divergence of the magnetic field lines near the target may play an important role in determining the column radial dimension. Further experiments and analysis are therefore suggested in order to optimize the vacuum-arc centrifuge parameters and for development of such devices into practical isotope separators. The results of the steady state analysis presented here are in good agreement with experimental findings for the plasma behavior in a vacuum-arc centrifuge, as the plasma column reaches an asymptotic, quasi-steady behavior at about 70cm downstream from the cathode. A time-dependent analysis can shed some light on how this quasi--equilibrium is attained within a few ion rotation orbits about the column axis.

The model described here can be directly applied to predict the behavior of rotating plasmas in the vacuum-arc centrifuge developed at INPE, considering parameters specific for each type of plasma being investigated.

REFERENCES

ALFVÉN, H. (1960). *Rev. Mod. Phys.*, 32, 710.

BONNEVIER, B. (1971). *Plasma Phys.*, 13, 763.

BONNEVIER, B. (1966). *Arkiv Fysik*, 33, 255.

BRAND, G.F.; JAMES, B.W. and WALSH, C.J. (1979). *J. Phys. D*, 12, 1495.

DEL BOSCO, E.; DALLAQUA, R.S.; LUDWIG, G.O. and BITTENCOURT, J.A.(1986). *Phys. Lett.*, to be submitted.

DEL BOSCO, E.; DALLAQUA, R.S. and LUDWIG, G.O. (1985). *Rev. Brasil. Apl. Vac.*, 5, 160.

DEL BOSCO, E. and LUDWIG, G.O. (1982). *Rev. Brasil. Fís.*, Vol. Esp. II (Latin-American Workshop on Plasma Physics and Controlled Nuclear Fusion Research), 493.

FAHLESON, U.V. (1961). *Phys. Fluids*, 4, 123.

GEVA, M.; KRISHNAN, M. and HIRSHFIELD, J.L. (1984). *J. Appl. Phys.*, 56, 1398.

GEVA, M.; KRISHNAN, M. and HIRSHFIELD, J.L. (1981). *Nucl. Instrum. Meth.*, 186, 183.

HELLER, H. and SIMON, M. (1974). *Phys. Lett.*, 50A, 139.

JAMES, B.W. and SIMPSON, S.W. (1978). *Plasma Phys.*, 20, 759.

JAMES, B.W. and SIMPSON, S.W. (1974). *Phys. Lett.*, 46A, 347.

KANEKO, O.; SASAKI, S. and KAWASHIMA, M. (1978). *Plasma Phys.*, 20, 1167.

KRISHNAN, M.; GEVA, M. and HIRSHFIELD, J.L. (1983). *Phys. Fluids*, 26, 2676.

KRISHNAN, M.; GEVA, M. and HIRSHFIELD, J.L. (1981). *Phys. Rev. Lett.*, 46, 1.

LEHNERT, B. (1971). *Nucl. Fusion*, 11, 485.

LEHNERT, B. (1960). *Rev. Mod. Phys.*, 32, 1012.

MCKENZIE, J.F. and VARMA, R.K. (1981). *J. Plasma Phys.*, 25, 491.

PRASAD, R.R. and KRISHNAN, M. (1986). *Rev. Sci. Instrum.*, 57, 74.

SLEPIAN, J. (1955). *J. Appl. Phys.*, 26, 1283.

SOCKOL, P.M. (1968). *Phys. Fluids*, 11, 637.

WIJNAKKER, M.M.B. and GRANNEMAN, E.H.A. (1980). *Z. Naturforsch*, 35A, 883.